OXFORD

Human Molecular Genetics, 2016, Vol. 25, No. 17 3699–3714

doi: 10.1093/hmg/ddw217
Advance Access Publication Date: 27 July 2016
Original Article

ORIGINAL ARTICLE

Coordinated movement, neuromuscular synaptogenesis and trans-synaptic signaling defects in *Drosophila* galactosemia models

Patricia P. Jumbo-Lucioni[1], William M. Parkinson[1], Danielle L. Kopke[1] and Kendal Broadie[1,2,*]

[1]Department of Biological Sciences and [2]Kennedy Center for Research on Human Development, Vanderbilt University, Nashville, TN, USA

*To whom correspondence should be addressed at: Kendal Broadie, VU Station B, Box 35-1634, Nashville, Tennessee 37235-1634, TN, USA. Tel: +615-936-3937; Fax: +615-936-0129; Email: kendal.broadie@vanderbilt.edu

Abstract

The multiple galactosemia disease states manifest long-term neurological symptoms. Galactosemia I results from loss of galactose-1-phosphate uridyltransferase (GALT), which converts galactose-1-phosphate + UDP-glucose to glucose-1-phosphate + UDP-galactose. Galactosemia II results from loss of galactokinase (GALK), phosphorylating galactose to galactose-1-phosphate. Galactosemia III results from the loss of UDP-galactose 4'-epimerase (GALE), which interconverts UDP-galactose and UDP-glucose, as well as UDP-N-acetylgalactosamine and UDP-N-acetylglucosamine. UDP-glucose pyrophosphorylase (UGP) alternatively makes UDP-galactose from uridine triphosphate and galactose-1-phosphate. All four UDP-sugars are essential donors for glycoprotein biosynthesis with critical roles at the developing neuromuscular synapse. *Drosophila* galactosemia I (*dGALT*) and II (*dGALK*) disease models genetically interact; manifesting deficits in coordinated movement, neuromuscular junction (NMJ) development, synaptic glycosylation, and Wnt *trans*-synaptic signalling. Similarly, *dGALE* and *dUGP* mutants display striking locomotor and NMJ formation defects, including expanded synaptic arbours, glycosylation losses, and differential changes in Wnt *trans*-synaptic signalling. In combination with *dGALT* loss, both *dGALE* and *dUGP* mutants compromise the synaptomatrix glycan environment that regulates *Wnt trans*-synaptic signalling that drives 1) presynaptic Futsch/MAP1b microtubule dynamics and 2) postsynaptic Frizzled nuclear import (FNI). Taken together, these findings indicate UDP-sugar balance is a key modifier of neurological outcomes in all three interacting galactosemia disease models, suggest that Futsch homolog MAP1B and the Wnt Frizzled receptor may be disease-relevant targets in epimerase and transferase galactosemias, and identify UGP as promising new potential therapeutic target for galactosemia neuropathology.

Introduction

Galactose is metabolized in a series of reactions catalyzed by the three consecutive enzymes that comprise the Leloir pathway: galactokinase (GALK1), galactose-1-phosphate uridyltransferase (GALT) and UDP-galactose 4' epimerase (GALE). Human deficits in the activity of any of these enzymes result in galactosemia disease states. Classic galactosemia (CG, OMIM 230400) results from loss of GALT activity (1) the second pathway enzyme (Figure 1A) . After GALK1 phosphorylation, GALT converts galactose-1-phosphate and uridine diphosphate-glucose (UDP-glucose) into glucose-1-phosphate and UDP-galactose. GALE catalyzes the final step converting UDP-galactose to UDP-glucose, as well as their N-acetylated forms:

Received: January 21, 2016. **Revised:** June 28, 2016. **Accepted:** June 30, 2016

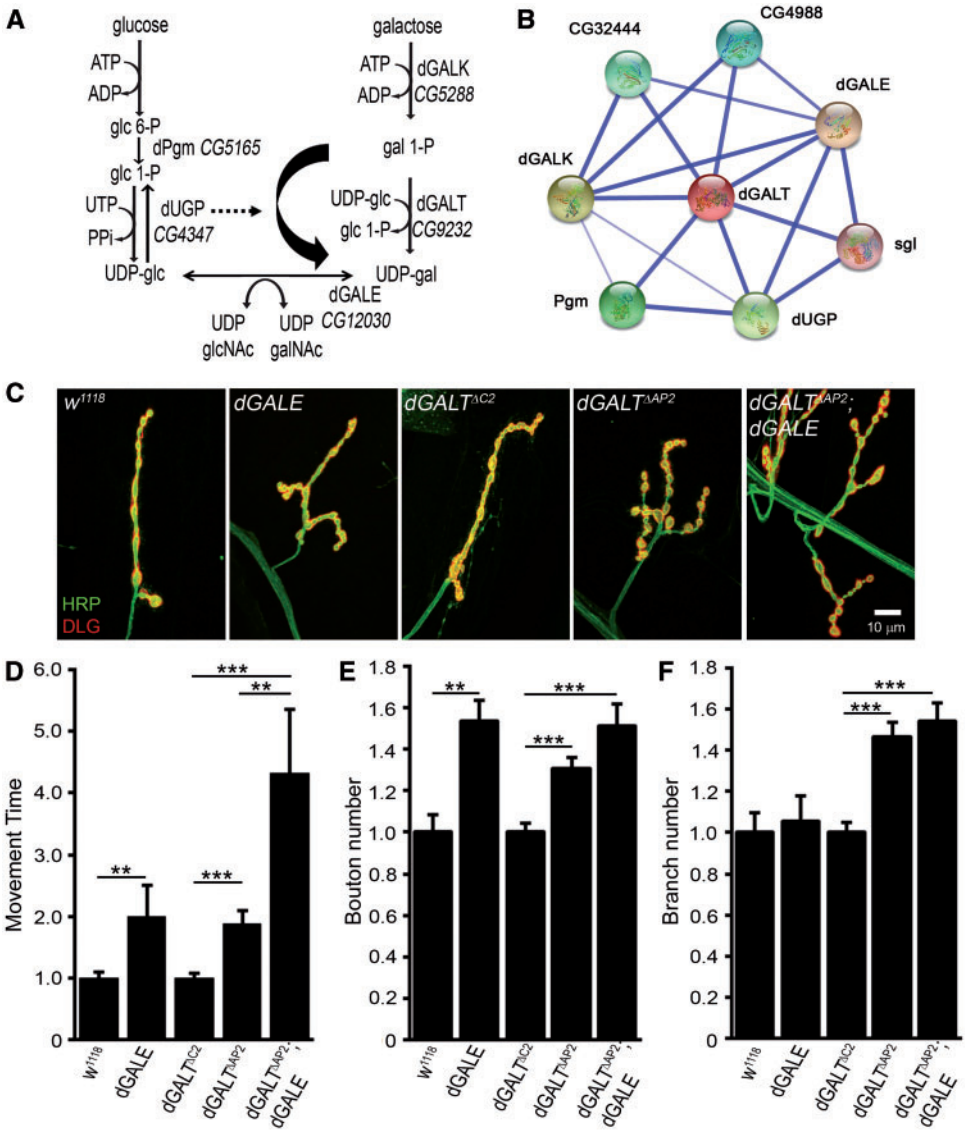

Figure 1. *dGALE* phenocopies *dGALT* and co-removal worsens coordinated movement. (**A**) Schematic diagram of glucose/galactose pathways showing targeted *dGALT*, *dGALE* and *dUGP* gene products. (**B**) The *dGALT* interaction network generated with the Search Tool for Retrieval of Interacting Genes (STRING). Line thickness represents the strength of predicted interactions. (**C**) Representative NMJs co-labelled with anti-horseradish peroxidase (HRP; green) and anti-Discs Large (DLG; red) in background control (w^{1118}) and homozygous *dGALE* mutant ($dGALE^{h}$); precise excision *dGALT* control ($dGALT^{\Delta C2}$), homozygous *dGALT* null mutant ($dGALT^{\Delta AP2}$) and double mutant ($dGALT^{\Delta AP2}$; *dGALE*) combinations. Movement time for coordinated roll-over behaviour. (**D**) NMJ bouton. (**E**) and branch. (**F**) number in the same genotypes, normalized to respective genetic controls. Sample size: ≥8 animals per genotype. Error bars show SEM with significance indicated as $^{*}P \leq 0.05$, $^{**}P \leq 0.01$ and $^{***}P \leq 0.001$.

UDP N-acetylglucosamine (UDP-GlcNAc) to UDP N-acetylgalactosamine (UDP-GalNAc; Figure 1A) (2). These four UDP sugars are critical for the biosynthesis of glycoproteins and proteoglycans (3,4), which heavily populate the cell surface and secreted surroundings, including the extracellular synaptomatrix of the synaptic cleft and perisynaptic space (5). UDP-glucose pyrophosphorylase (UGP2) synthesizes UDP-glucose from glucose-1-phosphate and UTP, and alternatively forms UDP-galactose from galactose-1-phosphate and UTP (6), independent of GALT activity (Figure 1A). UGP2 is present in a wide array of organisms (7,8) since UDP-glucose, the active form of glucose, is a central player in almost all living systems. The dual roles of UGP2 in both glucose and galactose metabolic pathways underscore its central importance as an alternative enzymatic route in galactosemia patients (9).

Classic galactosemia (aka galactosemia I) is the second most common inherited metabolic disorder among US children (10), and the most frequent and clinically severe galactosemia disease state (11). Galactosemia II (OMIM 230200) results from loss of GALK1, which we have previously established as a genetically interacting condition (12). Galactosemia III (OMIM 230250) results from loss of GALE, and is the rarest and least well understood form of galactosemia (13). Galactosemia I is often detected pre-symptomatically in newborn screening, and lifelong dietary galactose withdrawal, the current standard of care, resolves at least the acute life-threatening symptoms. Dietary intervention also resolves early onset cataracts in galactosemia II, the main disease symptom (14,15). However, long-term neurological symptoms arise in maturing galactosemia patients, including movement defects, speech delay and cognitive

disability (11), which are not prevented by dietary galactose control. Moreover, galactosemia III is a continuum disorder that can present life-threatening symptoms and long-term neurodevelopmental sequelae (11,16), and galactose restriction is particularly problematic as GALE plays a pivotal role maintaining UDP sugar balance during the synthesis of glycoproteins. Thus, the current treatment for GALE-associated galactosemia requires a balance between restricting galactose and providing enough for UDP sugar synthesis (17).

A large body of research documents glycosylation defects in galactosemia patients (18–20). Previous studies reveal conserved glycosylation defects in the *Drosophila* galactosemia I model (*dGALT* null mutant), and show the correction of glycosylation defects with co-removal of *dGALK*, in the *Drosophila* galactosemia II model (12). *dGALT* nulls exhibit severe coordinated locomotor movement deficits, as well as underlying strikingly overelaborated neuromuscular junction (NMJ) synaptic architecture. Importantly, the disease state is restricted to morphological defects without changes in neurotransmission strength. Assaying the heavily-glycosylated NMJ synaptomatrix with a series of lectin probes shows profound differences in synaptic glycan landscape dependent on *dGALT* activity (12). In particular, the heparan sulphate proteoglycan (HSPG) Wnt co-receptor Dally-like protein (Dlp) is lost from the NMJ synaptic interface, together with extracellular accumulation of the Wingless (Wg) Wnt glycoprotein signalling ligand. Wg signalling via its Frizzled 2 (Fz2) receptor modulated by the Dlp co-receptor is a key *trans*-synaptic signalling pathway regulating NMJ synaptogenesis (21–23). Importantly, coordinated movement, NMJ development, synaptomatrix glycan composition and Wnt pathway defects in the *Drosophila* galactosemia I disease model are all significantly corrected by co-removal of *dGALK* (12). This work strongly suggests NMJ glycan-dependent Wnt signalling defects as a basis for movement deficits in galactosemia I.

In the current study, we set forth to characterize a *Drosophila* galactosemia III model (*dGALE* mutant), as well as test the bypass pathway (*dUGP* mutant) for galactose metabolism. We find both *dGALE* and *dUGP* phenocopy coordinated movement deficits and impaired NMJ synaptogenesis characterizing *dGALT*. Loss of *dGALE* elevates neurotransmission strength, which is further heightened by co-removal of *dGALT*. Defects in all three mutants include synaptomatrix glycosylation losses, elevated synaptic bouton formation and differences in the core Wg/Fz2/Dlp *trans*-synaptic signalling pathway components. Both *dGALT* and *dGALE* display increased Futsch/MAP1b microtubule remodeling in the presynaptic neuron, whereas *dUGP* exhibits elevated Frizzled nuclear import (FNI) in the postsynaptic muscle. These new findings reveal 1) key glycosylation pathway modifiers of Wnt *trans*-synaptic signalling, and 2) identify two new diseases-relevant targets, Futsch/MAP1b and Wnt Frizzled receptor, for intervention in galactosemia-associated neuropathology. Both *dGALE* and *dUGP* interact with *dGALT*, modifying behavioural deficits and changes in synaptic architecture in the *Drosophila* galactosemia I model. Synaptic glycosylation losses, particularly of N-acetylgalactosamine residues, are exacerbated. These findings indicate that differential glycosylation at the NMJ synaptomatrix modulates neurological movement outcomes in interacting galactosemia disease states, and further suggest UGP as a promising new therapeutic target for galactosemia treatment.

Results

Neuronal *dGALE* loss worsens behavioural outcomes in *dGALT* null mutants

Movement defects are common among *GALT*-deficient galactosemia patients (24–28). Similarly, *dGALT* is necessary for proper coordinated movement in the *Drosophila* disease model, and *dGALK* co-removal corrects this behavioural deficit (12). In the galactose pathway, *dGALE* intersects with *dGALT* downstream (Figure 1A), and the Search Tool for Retrieval of Interacting Genes (STRING) (29) identified *dGALE* as a promising candidate interactor (Figure 1B), consistent with previous evidence of an interactive relationship (30). GALE-deficient galactosemia patients also exhibit deficits in coordinated motor skills that appear early in development (31,32). However, most of the severe patient cases arise from consanguineous parents, which raises the possibility that homozygosity of autosomal recessive alleles other than *GALE* may underlie some of the severe movement symptoms reported in galactosemia III (31). Animal models have shown GALE activity is essential for viability (33) and normal development (34,35), but movement phenotypes have not been investigated despite evidence of *GALE* expression in neurons and muscle in *C. elegans* (35). We therefore set out to assay coordinated movement in our *Drosophila* model. Null *dGALE* mutants manifest early lethality, confirming that *dGALE* is essential for viability, and therefore viable $dGALE^{h}$ hypomorphic mutants with residual ~8% dGALE activity (34) were tested.

A well-established test for *Drosophila* coordinated movement is the larval rollover assay, which requires a complex set of integrated behaviours to be properly executed, as previously described (12). In this assay, wandering L3 larvae (wL3) are placed in an inverted position and the time to righting is measured. Compared to genetic background controls (w^{1118}) showing rapid and well-coordinated movement (8.2 ± 1.09 s, $n = 24$ animals), $dGALE^{h}$ mutants exhibit clearly uncoordinated and >2-fold slower responses (17.7 ± 5.64 s, $n = 23$, $P = 0.01$; Figure 1D). Mutant larvae make several attempts to twist and roll before they successfully right themselves. Similarly, as previously reported (12), *dGALT* null ($dGALT^{\Delta AP2}$) animals are significantly movement impaired, also manifesting ~2-fold slower righting time compared to precise-excision genetic background ($dGALT^{\Delta C2}$) matched controls ($n = 36,38$; $P < 0.001$; Figure 1D). We hypothesized *dGALE* would exacerbate *dGALT* movement impairments since *dGALE* synthesizes UDP-sugar precursors when limited by *dGALT* deficiency (Figure 1A). Consistently, the double mutants (homozygous $dGALT^{\Delta AP2}$; $dGALE^{h}$) manifest >2- and >4-fold longer period to complete the coordinated movement (56.3 ± 17.77 s, $n = 15$) compared to *dGALT* single mutants ($P < 0.01$) and genetic controls ($P < 0.001$, Figure 1D), respectively. Our findings suggest that *dGALT* and *dGALE* contribute equally to the control of coordinated movement, and that loss of the two genes has an additive effect on coordinated movement deficits.

To test the cellular requirements for *dGALE* in bilateral coordinated movement control, *dGALE* was knocked-down with transgenic RNAi (Figure 2). Like *dGALE* null mutants, ubiquitous (*UH1-Gal4*) *dGALE* knockdown results in 100% early lethality, and therefore could not be assayed. Like the $dGALE^{h}$ mutants, targeted neuronal *dGALE* RNAi (*elav*-Gal4 > *dGALE-RNAi*) also results in overtly uncoordinated animals, which likewise manifest >2-fold slower roll-over behaviour (18.7 ± 1.96 s, $n = 16$) compared to their driver alone (*elav*-Gal4/+) genetic controls

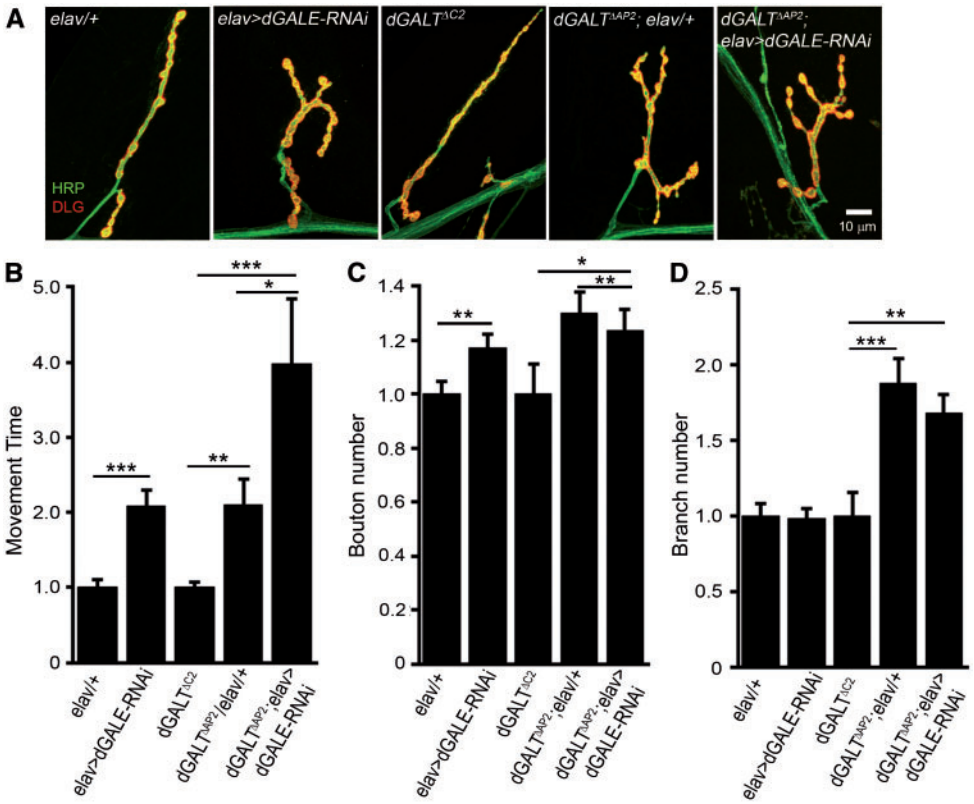

Figure 2. Targeted neuronal *dGALE* knockdown also phenocopies *dGALT* mutants. (**A**) Representative NMJs co-labelled with presynaptic anti-HRP (green) and postsynaptic anti-DLG (red) in driver alone controls (*elav-Gal4/+*), neuronal-targeted *dGALE* RNAi (*elav*-Gal4>*dGALE-RNAi*); precise excision *dGALT* controls ($dGALT^{C2}$), *dGALT* nulls with driver alone ($dGALT^{\Delta AP2}$; *elav-Gal4/+*), and the double mutant animals ($dGALT^{\Delta AP2}$; *elav*-Gal4>*dGALE-RNAi*). Movement time for coordinated roll-over behaviour. (**B**) NMJ bouton. (**C**) and branch. (**D**) number in the same genotypes, normalized to respective genetic controls. Sample size: ≥10 animals for each genotype. Error bars show SEM with significance; $^{*}P \leq 0.05$, $^{**}P \leq 0.01$ and $^{***}P \leq 0.001$.

(9.0 ± 0.94 s, $n = 14$, $P = 0.0002$; Figure 2B). Similarly, targeted muscle *dGALE* RNAi (*24B*-Gal4 > *dGALE-RNAi*) causes >2-fold slower rollover (10.4 ± 1.64 s, $n = 24$) compared to genetic controls (*24B*-Gal4/+, 4.7 ± 0.46 s, $n = 28$, $P = 0.002$). These findings identify a neuronal and muscle *dGALE* requirement for properly controlled coordinated movement. Similar to the above *dGALT*; *dGALE* double mutant condition, targeted *dGALE* neuronal knockdown in the *dGALT* null background (homozygous $dGALT^{\Delta AP2}$; *elav*-Gal4 > *dGALE-RNAi*) causes further slowing of roll-over time (34.6 ± 11.46 s, $n = 25$) compared to *dGALT* with driver alone ($dGALT^{\Delta AP2}$; *elav*-Gal4/+) animals (15.7 ± 1.61 s, $n = 29$), as well as precise excision control ($dGALT^{\Delta C2}$) animals (8.8 ± 0.77 s, $n = 51$, $P < 0.001$; Figure 2B). Conversely, postsynaptic targeted *dGALE* knockdown in the *dGALT* null background (homozygous $dGALT^{\Delta AP2}$; *24B*-Gal4 > *dGALE-RNAi*) does not further compromise locomotor coordination (20.8 ± 2.14 s, $n = 22$) compared to *dGALT* alone ($dGALT^{\Delta AP2}$; *elav*-Gal4/+: 18.4 ± 2.67 s, $n = 9$). Taken together, these results demonstrate that neuronal and muscle *dGALE* both contribute to properly controlled coordinated movement, and that presynaptic, but not postsynaptic, *dGALE* is a strong genetic modifier of d*GALT* disease model behavioural deficits in an additive manner. As these movement defects have been closely associated with changes in NMJ morphological development (12), we next examined the synaptic architecture in d*GALE* single mutants and in *dGALE; dGALT* double mutant animals.

Neuronal *dGALE* regulates neuromuscular synaptogenesis and transmission strength

We conducted a *Drosophila* glycogene screen using transgenic RNAi knockdown of a wide range of N/O-linked glycans, glycosaminoglycans, glycosyltransferases and glycan-binding lectins to test effects on NMJ structure and function (21). This screen identified *dGALT* as a strong negative regulator of NMJ structural synaptogenesis, but not functional differentiation, and we subsequently confirmed that *dGALT* acts to restrict terminal arbour branching and synaptic bouton formation (12). Since defects in NMJ morphogenesis have been shown to underlie locomotor deficits (12,36,37), we hypothesized that similar defects could account for the movement limitations occurring in the absence of neuronal *dGALE*, as well as for the worsening of movement deficits in *dGALE; dGALT* double mutant conditions. To assay synapse architecture, muscle 4 NMJs from wL3 animals were co-labelled with presynaptic anti-horseradish-peroxidase (HRP, green) and postsynaptic anti-Discs Large (DLG, red) in single and double mutant animals. Synaptic boutons (>1μm in minimum diameter) and branches (axonal processes with >2 boutons) were counted. Representative images and quantification for mutant and control genotypes are shown in Figures 1 and 2.

The synaptic bouton number is increased by >50% in $dGALE^{h}$ mutants (30.3 ± 2.0, $n = 8$ animals) compared to w^{1118} genetic background controls (19.7 ± 1.7, $n = 10$, $P = 0.002$; Figure 1E).

Targeted neuronal *dGALE* knockdown (*elav*-Gal4 > *dGALE*-RNAi) animals similarly show a significant, although smaller (~17%), increase in bouton number compared to driver alone (*elav*-Gal4/+) genetic controls ($n = 13,16$; $P = 0.01$; Figure 2C). While both *dGALE* mutants and neuron-targeted *dGALE*-RNAi animals display obvious NMJ overelaboration (Figures 1C, 2A), muscle-targeted *dGALE*-RNAi does not cause a detectable change in synaptic architecture or a significant increase in synaptic bouton number compared to genetic controls (25.1 ± 1.1 boutons, $n = 35$ vs. 26.9 ± 1.2 boutons, $n = 35$, respectively). These findings show a specific requirement for *dGALE* in the neuron, in this case to restrict NMJ synaptogenesis. In double mutant conditions, the NMJ architectural complexity characterizing *dGALT* nulls is exacerbated by simultaneously reducing *dGALE* activity (Figure 1C). Compared with the significantly greater number of boutons in *dGALT* single mutants (34.5 ± 1.6, $n = 33$), double mutant synapses (homozygous $dGALT^{\Delta AP2}$; $dGALE^{h}$) develop ~50% and ~20% more boutons (39.8 ± 2; $n = 40$), compared to genetic control ($dGALT^{\Delta C2}$) (26.4 ± 1.3; $n = 26$, $P < 0.001$; Figure 1E) and *dGALT* single mutants (Figure 1E), respectively. Neuronal *dGALE* knockdown in the *dGALT* null background did not further increase NMJ structural complexity (Figure 2C,D). Single $dGALE^{h}$ and *dGALE-RNAi* also did not increase synaptic branching (Figures 1F,2D), in contrast to *dGALT* mutants (3.8 ± 0.2, $n = 33$) which increased synaptic branching compared to controls (2.6 ± 0.1, $n = 24$, $P < 0.001$; Figure 1F). There is a tendency for branching to increase further in *dGALE; dGALT* double mutants (4 ± 0.2, $n = 40$), but the effect is not significant (Figure 1F).

To test NMJ functional differentiation, we performed two-electrode voltage clamp (TEVC) electrophysiological recordings (12). The innervating motor nerve was stimulated with a glass suction electrode while recording from the voltage-clamped muscle 6. Excitatory junctional current (EJC) records were made at 0.2 Hz frequency with 0.5 ms duration stimuli at a suprathreshold voltage. ≥25 NMJs from ≥10 different wL3 animals were recorded from each of three genotypes: genetic background control (w^{1118}), *dGALE* alone ($dGALE^{h}$) and a double mutant in combination with *dGALT* ($dGALT^{\Delta AP2}$; $dGALE^{h}$). Neurotransmission strength is very obviously elevated with loss of *dGALE* activity (Figure 3A). Mean EJC amplitudes significantly increased in mutants compared to control (313.3 ± 15.6 nA vs. 241.4 ± 8.6 nA; $P \leq 0.001$; Figure 3B). Strikingly, the double mutant combination exhibits further heightened neurotransmission (Figure 3A). Mean EJC amplitudes significantly increased in double mutants ($dGALT^{\Delta AP2}$; $dGALE^{h}$: 413.2 ± 12.4 nA) compared to both w^{1118} control ($P \leq 0.001$, Figure 3B) and single *dGALE* mutants ($P \leq 0.001$, Figure 3B). In summary, these results show that *dGALE* is a strong genetic modulator of both neuromuscular structural synaptogenesis and functional differentiation alone and in combination with *dGALT* loss at the NMJ synapse.

dGALT genetic modifier *dUGP* regulates coordinated movement and NMJ architecture

STRING analyses (29) further identified *dUGP* as a second highly-associated *dGALT* interactor (Figure 1A,B). In *Drosophila*, *CG4347* encodes UDP-glucose pyrophosphorylase (EC 2.7.7.9) as the only enzyme capable of producing UDP-glucose from glucose-1-P and UTP (38–41) (Figure 1A). Like *dGALE*, *dUGP* is essential for viability and, consistently, no human patients with *UGP* loss-of-function mutations have been reported. We therefore characterized two *dUGP* hypomorphic mutations ($dUGP^{1}$, $dUGP^{2}$) generated by transposable element insertion (42). Neither mutant is homozygous viable, but viability is restored with significantly reduced survival in heteroallelic combination ($dUGP^{1}/dUGP^{2}$). We first tested *dUGP* mutants for coordinated movement behaviour using the same larval roll-over assay as above. Compared to w^{1118} genetic background controls (7.6 ± 0.71 s, $n = 29$), $UGP^{1}/+$ (11.6 ± 1.33 s, $n = 15$, $P < 0.05$) and $UGP^{2}/+$ (16.0 ± 1.82 s, $n = 15$, $P < 0.001$) animals are both significantly slower and obviously less coordinated (Figure 4B). The coordinated movement time for $UGP^{1}/+$ is not significantly different from $UGP^{2}/+$, although $UGP^{2}/+$ appears qualitatively more behaviourally compromised. Combined $dUGP^{1}/dUGP^{2}$ mutants display a significant further reduction in coordinated movement (18.6 ± 1.73 s, $n = 15$) compared to single *dUGP* heterozygotes ($P < 0.05$) and w^{1118} controls ($P < 0.001$; Figure 4B). Ubiquitous *dUGP* knockdown (*UH1*-Gal4 > *dUGP-RNAi*) caused the strongest effect, with >2.5-fold longer time to upright position (25.2 ± 2.78 s, $n = 10$) compared to control (*UH1*-Gal4/+: 9.3 ± 1.47 s, $n = 9$, $P = 0.004$). Tissue-targeted neural (*elav*-Gal4 > *dUGP*-RNAi: 13.6 ± 1.82 s, $n = 29$, $P < 0.05$) and muscle (*24B*-Gal4 > *dUGP*-RNAi: 19.7 ± 4.40 s, $n = 12$, $P < 0.05$) knockdown both significantly impaired coordinated movement compared to the driver alone controls (*elav-Gal4*/+: 8.8 ± 0.70 s, $n = 23$; *24B-Gal4*/+: 8.2 ± 1.0 s, $n = 14$).

UGP2 *loss* causes a dramatic reduction in UDP-glucose, an essential precursor for the biosynthesis of proteoglycans (43), which are key components of the NMJ synaptomatrix and established regulators of NMJ development (5). Although UGP2 has a higher affinity for glucose-1-P, it also catalyzes UDP-galactose from galactose-1-P and UTP (6,9), particularly at the high galactose-1-P levels in *GALT*-deficient galactosemia patients (11). Thus, UGP2 represents an alternate GALT-independent pathway for galactose metabolism (9) (Figure 1A). We therefore hypothesized that *dUGP* loss would enhance behavioural impairments in *dGALT* mutants and produce an exacerbated phenotype. Since $dUGP^{1}/dUGP^{2}$ is the most severely impaired conditioned, coordinated movement was next assayed in the homozygous $dGALT^{\Delta AP2}$; $dUGP^{1}/dUGP^{2}$ combination (Figure 4B). As predicted, these double mutant animals are obviously less coordinated than either of the single mutant conditions, with a 2-fold slower roll-over time (44.1 ± 10.94 s, $n = 27$) compared to *dGALT* nulls alone (22.4 ± 2.53 s, $n = 23$, $P < 0.05$) and >4-fold change compared to genetic background controls (10.3 ± 0.90 s, $n = 50$, $P < 0.001$; Figure 4B). These results show that *dUGP* plays a particularly important role enabling coordinated movement, and that co-removal of *dUGP* and *dGALT* combinatorially further impairs the ability to move in a coordinated manner.

We next assayed NMJ synaptogenesis in *dUGP* mutants (Figure 4A). Like both *dGALT* and *dGALE* mutants, loss of *dUGP* causes NMJ overgrowth and structural overelaboration in $UGP^{1}/+$, $UGP^{2}/+$ and UGP^{1}/UGP^{2} mutants. Compared to the w^{1118} genetic background control (21.2 ± 1.0 boutons, $n = 22$), both $UGP^{1}/+$ (28.3 ± 2.1, $n = 12$, $P < 0.05$) and $UGP^{2}/+$ (30.7 ± 1.4, $n = 17$, $P < 0.01$), as well as $dUGP^{1}/dUGP^{2}$ (28.8 ± 2.7, $n = 6$, $P < 0.001$), develop significantly more synaptic boutons (Figure 4C). Synaptic branching tends to increase in all *dUGP* mutants, but is only significantly greater in $UGP^{1}/+$ (2.8 ± 0.2, $n = 12$) compared to w^{1118} genetic controls (2.3 ± 0.2, $n = 22$, $P < 0.05$; Figure 4D). Single *dGALT* nulls ($dGALT^{\Delta AP2}/dGALT^{\Delta AP2}$: 32.9 ± 1.9; $P < 0.05$, $n = 19$) and particularly, the double mutant combination ($dGALT^{\Delta AP2}/dGALT^{\Delta AP2}$; $dUGP^{1}/dUGP^{2}$: 35.7 ± 1.6; $P < 0.001$, $n = 29$) develop significantly more synaptic boutons compared to the $dGALT^{\Delta C2}$ precise excision controls (24.9 ± 1, $n = 22$; Figure 4C). Synaptic branching increases in $dGALT^{\Delta AP2}$ mutants (3.3 ± 0.3, $n = 19$)

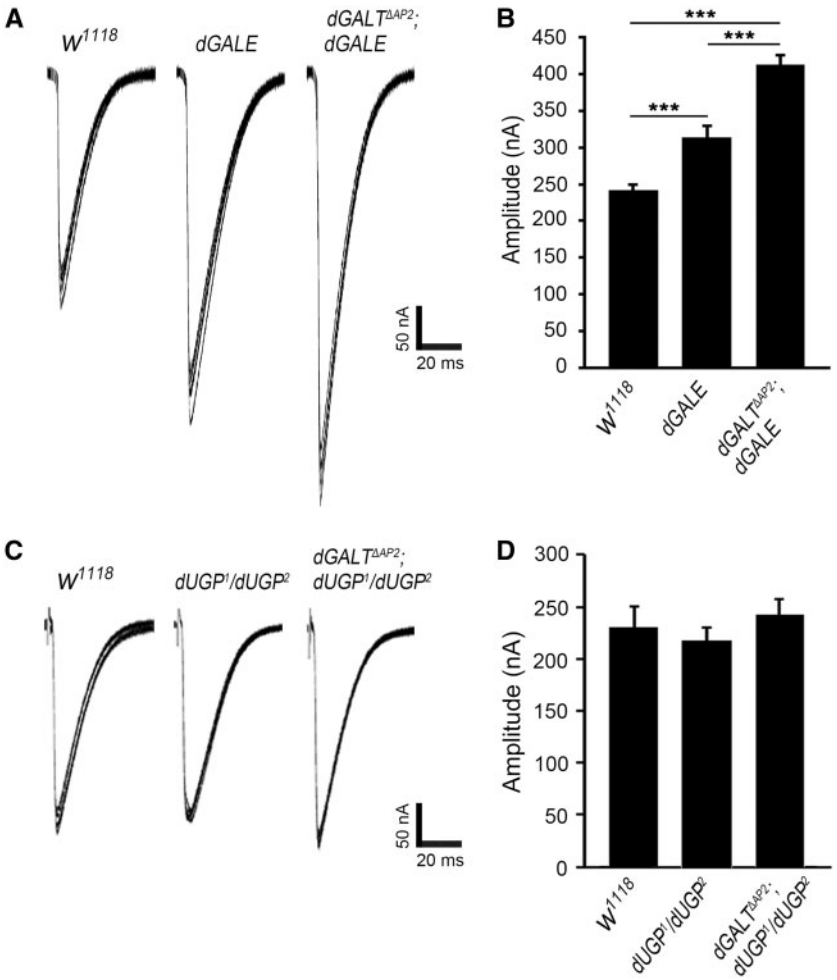

Figure 3. *dGALE* loss elevates transmission and *dGALT* co-removal worsens the defect. (**A**) Representative EJC traces from genetic background control (w^{1118}), *dGALE* single mutant ($dGALE^h$) and double mutant animals ($dGALT^{\Delta AP2}$; $dGALE^h$). (**B**) EJC peak amplitude quantification for all three genotypes. Sample size: ≥25 NMJs for each genotype. Error bars show SEM with significance indicated: ***P<0.001. (**C**) Representative EJC traces from control (w^{1118}), single *dUGP* mutant ($dUGP^1/dUGP^2$) and double mutant animals ($dGALT^{\Delta AP2}$; $dUGP^1/dUGP^2$). D) EJC peak amplitude quantification for all three genotypes. Sample size: ≥12 NMJs for each genotype. There is no significant differences.

compared to $dGALT^{\Delta C2}$ controls (2.7 ± 0.1, $n = 22$), but there is a further significant increase in branching in double mutants (3.9 ± 0.2, $n = 29$, $P < 0.001$; Figure 4D).Consistently, ubiquitous *dUGP* knockdown (*UH1*-Gal4 > *dUGP-RNAi*) significantly increases synaptic bouton (35.5 ± 1.56, $n = 11$, $P < 0.0003$) and branch (3.36 ± 0.20, $n = 11$, $P < 0.0017$) numbers compared to driver alone controls (*UH1*-Gal4/+: 25.2 ± 1.56, $n = 10$ and 2.25 ± 0.23, $n = 10$, respectively). However, structure is over-elaborated in pan-neuronal *dUGP*-knockdown animals (26.3 ± 1.0 boutons, $n = 10$, $P = 0.007$), although unaffected in muscle-targeted *dUGP-RNAi* larvae (25.4 ± 2.4 boutons, $n = 11$) compared to their appropriate controls (22 ± 1.1, $n = 12$ and 20.2 ± 1.4, $n = 15$, respectively).

As above, we next tested NMJ functional differentiation with TEVC electrophysiological recordings (Figure 3). ≥12 NMJs from ≥6 different wL3 animals were recorded from each of three genotypes: genetic background control (w^{1118}), *dUGP* transheterozygotes ($dUGP^1/dUGP^2$) and double mutant animals ($dGALT^{\Delta AP2}$; $dUGP^1/dUGP^2$). Unlike *dGALE*, neurotransmission strength is closely comparable between all three genotypes (Figure 3C). Mean EJC amplitudes from single mutants (219.35 ± 12.60 nA) are not significantly different from w^{1118} control (230.36 ± 19.81 nA) or the double mutant combination (242.58 ± 15.09 nA, $P > 0.05$, Figure 3D). Taken together, these results show that *dUGP* is important for coordinated movement and neuromuscular structural synaptogenesis, but is not detectably required for synapse function. These findings show that co-removal of *dUGP* and *dGALT* interact to modify the severity of behavioural and structural mutant phenotypes. Since there is extensive evidence showing synaptic glycosylation restricts NMJ morphogenesis (12,21,22), we next proceeded to examine the synaptic glycan environment in single and double mutant combinations.

dGALE and *dUGP* both shape NMJ synaptomatrix glycan composition

GALE plays a crucial role maintaining UDP-sugar balance for glycosylation (2), with a primarily role in UDP-galNAc biosynthesis. Unlike UDP-glc and UDP-glcNAc, UDP-galNAc cannot be synthesized by a GALE-independent pathway (Figure 1A). Indeed, recent studies reveal that GALE loss-of-function in *C. elegans* causes a strong reduction of UDP-galNAc levels

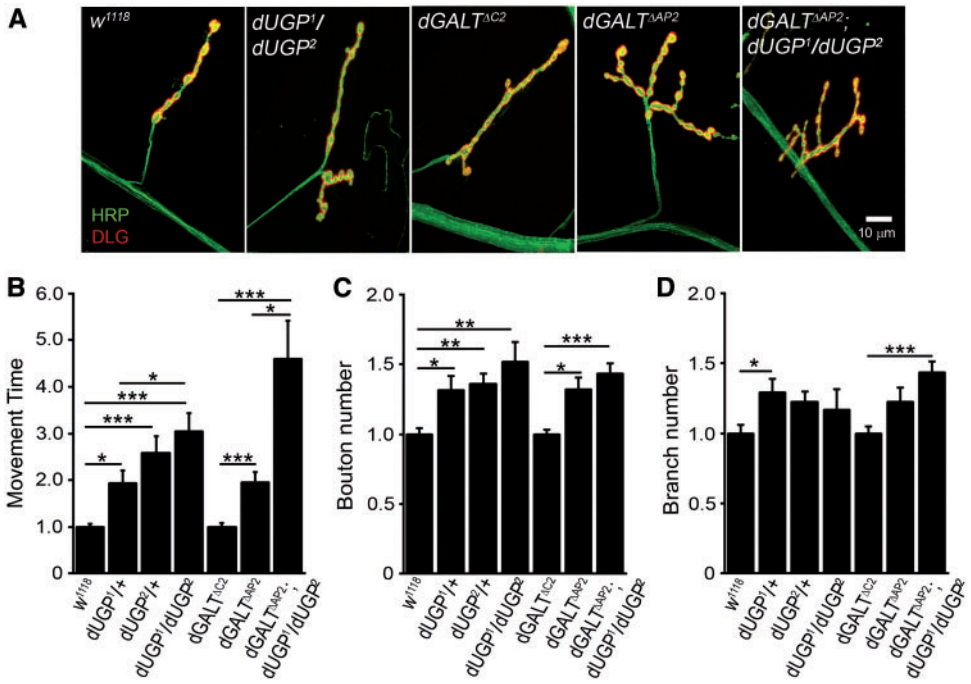

Figure 4. *dUGP* phenocopies *dGALT* and co-removal worsens coordinated movement. (**A**) Representative NMJs imaged with anti-HRP (green) and anti-DLG (red) in genetic control (w^{1118}), *dUGP* mutant ($dUGP^1/dUGP^2$); precise excision control ($dGALT^{\Delta C2}$), *dGALT* null ($dGALT^{\Delta AP2}$), and double mutant combinations ($dGALT^{\Delta AP2}$; $dUGP^1/dUGP^2$). Movement time for coordinated roll-over behaviour (**B**), NMJ bouton (**C**) and branch (**D**) number in the same genotypes, normalized to respective genetic controls. Sample size: ≥15 animals per genotype. Error bars show SEM with significance indicated: *P≤0.05, **P≤0.01 and ***P≤0.001.

accompanied by developmental defects unique to this UDP-sugar (35). We previously found similar glycan losses at the NMJ synaptomatrix in the absence of *dGALT* (12). Since this is the only glycan deficit corrected by transgenic *hGALT* expression in the *dGALT* null background (12), it provides a potential mechanistic basis for the coordinated movement and morphological synaptogenesis defects in this disease model. We hypothesized that *dGALE* deficiency, like loss of *dGALT*, would compromise galNAc abundance in the NMJ synaptomatrix in the new *Drosophila* epimerase galactosemia model, driving the synaptogenesis and movement deficits in *dGALE* mutants. To test this hypothesis, we first probed with *Wisteria floribunda* lectin (WFA, green) to label terminal galNAc residues in NMJs marked with Fasciclin-II (FasII, red). Representative images and data summary are shown in Figure 5.

The synaptic marker FasII does not vary significantly between tested genotypes, comparing w^{1118} genetic background control and $dGALE^h$ mutant NMJs (Figure 5A). In sharp contrast, while w^{1118} control NMJs ($n=38$) are very highly enriched with WFA-labelled galNAc residues, $dGALE^h$ synapses ($n=10$) show a dramatic ∼60% loss of WFA label ($P<0.001$; Figure 5A,C). To test whether *dGALT* co-removal would worsen the phenotype, *dGALT*; *dGALE* double mutants were next examined. The $dGALT^{\Delta AP2}$ single mutant decreases WFA labelling by ∼25% compared to precise controls ($n=42,46$; $P<0.001$; Figure 5A,C), and the double mutants ($dGALE^h/dGALE^h$; $dGALT^{\Delta AP2}/dGALT^{\Delta AP2}$) exhibit a further ∼35% reduction, significantly different from the single mutant condition ($dGALT^{\Delta AP2}/dGALT^{\Delta AP2}$, $P<0.05$; Figure 5C). Fucosylation defects are also reported in galactosemia (44), and the *Drosophila dGALT* disease model manifests a loss of anti-HRP labelling at the NMJ (12), a commonly employed synaptic marker recognizing α1,3-fucosylation. We therefore hypothesized *dGALE* mutants would manifest a similar glycosylation defect that would be exacerbated by co-removal of *dGALT*. Consistently, $dGALE^h$ NMJs show significantly reduced HRP glycan levels compared to controls ($n=6,6$; $P=0.006$), similar to $dGALT^{\Delta AP2}$ NMJs compared to controls ($n=16,17$; $P<0.05$), with the *dGALE*; *dGALT* double mutants exhibiting a stronger ∼30% reduction in HRP glycan levels ($n=16$, $P<0.001$ compared to $dGALT^{\Delta C2}$; Figure 5D). These results show that *dGALE* and *dGALT* both shape the glycan composition of the developing NMJ synaptomatrix.

We next tested *dUGP* single and double mutants with the same WFA and HRP probes (Figure 5A,B). While WFA-labelling in single *dUGP* mutants ($UGP^1/+$, $n=8$; $UGP^2/+$, $n=9$) is not significantly different from matched controls ($n=26$), the stronger UGP^1/UGP^2 *combination* shows a ∼40% reduction in WFA-labelled galNAc residues ($n=9$, $P<0.01$; Figure 5C). The $dGALT^{\Delta AP2}$ single mutant shows a ∼25% decrease ($n=42$) compared to controls ($n=46$, $P<0.001$; Figure 5C), and the double mutants ($dGALT^{\Delta AP2}/dGALT^{\Delta AP2}$; $dUGP^1/dUGP^2$) exhibit a further decrease in WFA labelling (∼30% reduction, $n=26$) compared to matched controls ($n=46$, $P<0.001$; Figure 5C). Anti-HRP labelling for fucosylation defects shows $dUGP^1/dUGP^2$ exhibits a ∼30% reduction ($n=10$) compared to w^{1118} genetic controls ($n=11$, $P<0.05$; Figure 5D). Both single $dGALT^{\Delta AP2}$ ($n=29$) and double $dGALT^{\Delta AP2}/dGALT^{\Delta AP2}$; $dUGP^1/dUGP^2$ ($n=18$) combinations show a similar ∼20% decrease in fucosylated residues at the NMJ, a significant decrease compared to controls ($n=30$; $P<0.05$ and $P<0.01$, respectively; Figure 5D). Taken together, these results show that *dGALE* and *dUGP* are strong genetic modifiers of NMJ synaptomatrix glycan composition, partially overlapping with *dGALT* requirements in synaptic glycosylation. Since we have previously found that these synaptomatrix defects alter NMJ

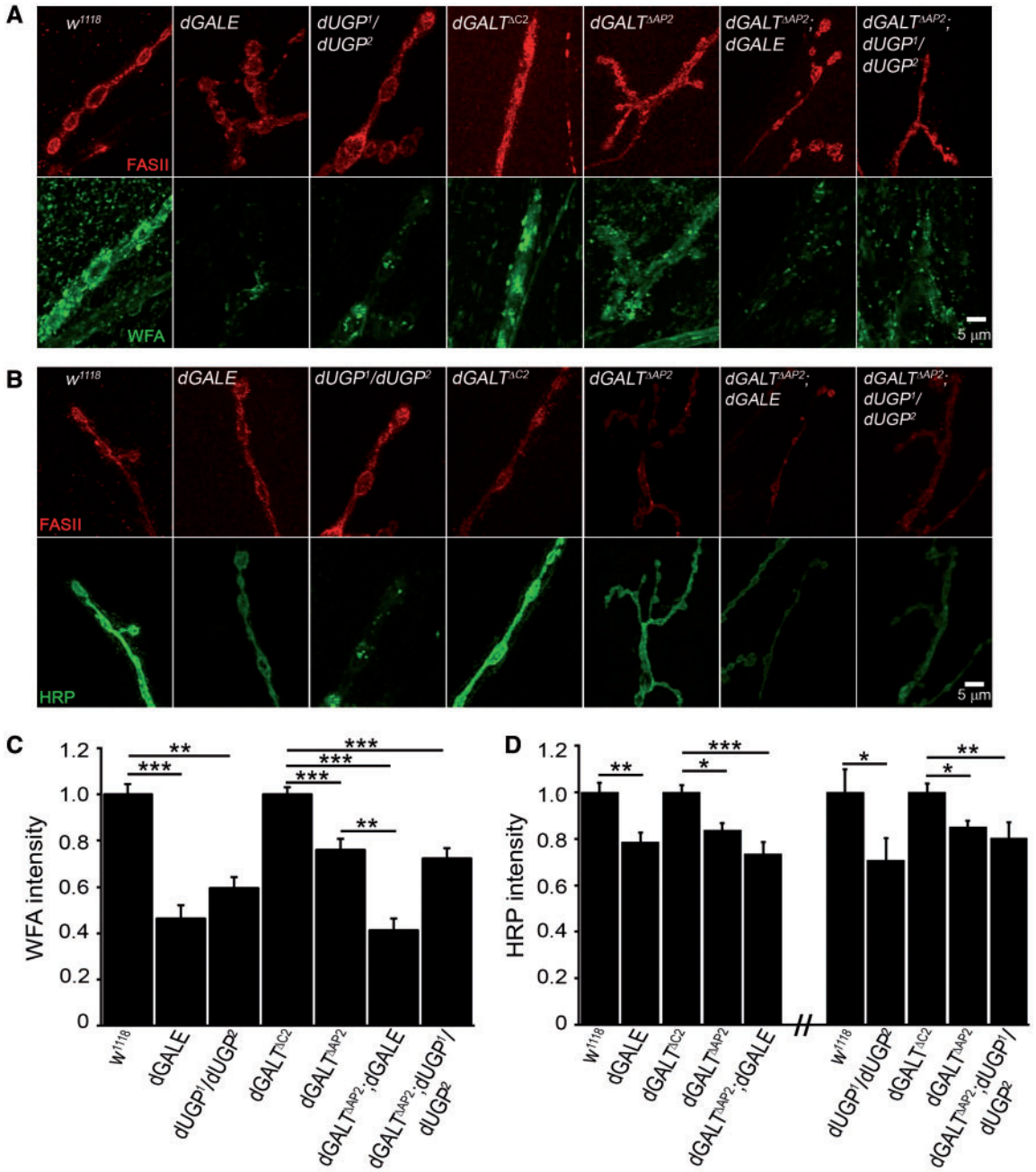

Figure 5. *dGALE* and *dUGP* mutants manifest glycan losses in the NMJ synaptomatrix. Representative NMJs co-labelled with anti-Fasciclin II (FASII, red). (**A**) *Wisteria floribunda* lectin (WFA, green) or (**B**) anti-horseradish peroxidase (HRP; green) in genetic control (w^{1118}), *dGALE* ($dGALE^{h}$) and *dUGP* ($dUGP^{1}/dUGP^{2}$) mutants; precise excision control ($dGALT^{C2}$), *dGALT* null ($dGALT^{\Delta AP2}$) and double mutant combinations ($dGALT^{\Delta AP2}$; *dGALE* and $dGALT^{\Delta AP2}$; $dUGP^{1}/dUGP^{2}$). Quantification of WFA. (**C**) and HRP. (**D**) intensities in the same genotypes, normalized to respective genetic controls. Sample size: ≥10 NMJs/animals per genotype. Error bars show SEM with significance indicated as *P≤0.05, **P≤0.01, ***P≤0.001 and ****P≤0.0001.

synaptogenesis via modulation of the Wg *trans*-synaptic signalling pathway (12), we next test whether this pathway is compromised in *dGALE* and *dUGP* single and double mutant combinations.

dGALE and *dUGP* both regulate wnt *trans*-synaptic signalling at the NMJ

The heavily-glycosylated cell surface and extracellular space modulates ligand-mediated signalling in normal and disease states (45), and the *Drosophila* NMJ glycosylated synaptomatrix has been repeatedly shown to fine-tune *trans*-synaptic signalling driving synaptogenesis (5,12,22). In the core Wnt pathway, UDP-sugar availability could also impact the glycosylation status of the secreted Wingless (Wg) glycoprotein ligand (46) and biosynthesis of Wg co-receptor HSPG Dlp (21), required for the optimal processing, availability and presentation of Wg within the synaptic cleft. We have previously shown that *dGALT* mutants increase Wg and reduce Dlp levels at the *Drosophila* NMJ (12). We therefore hypothesized that *dGALE* and *dUGP* mutants would likewise impact the Wg

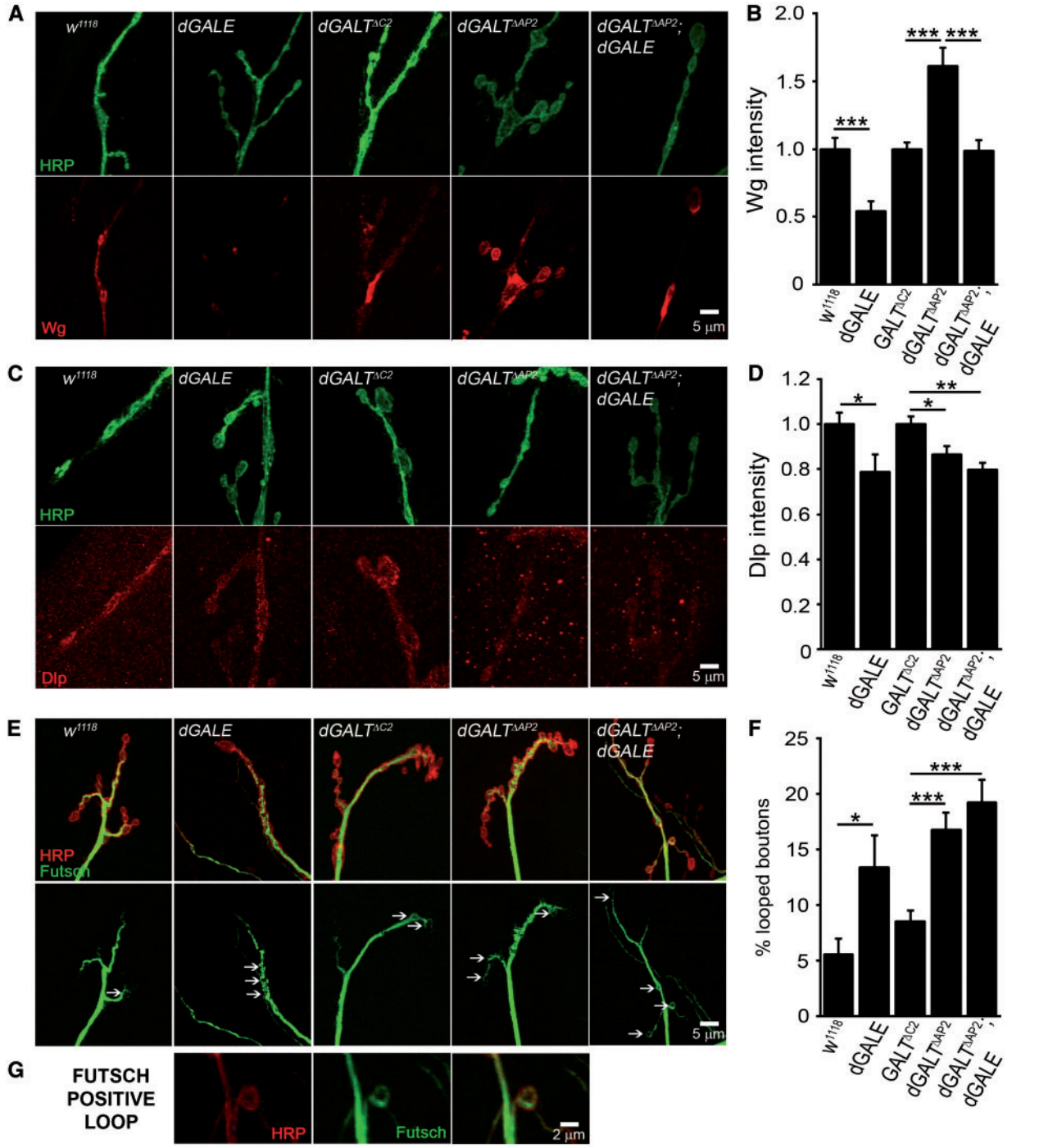

Figure 6. Presynaptic Wnt signalling upregulated in *dGALE* and *dGALT* double mutant. (**A**) Representative NMJ boutons co-labelled with anti-HRP (green) and anti-Wingless (Wg, red) in genetic control (w^{1118}) and *dGALE* mutant ($dGALE^{h}$); precise excision controls ($dGALT^{\Delta C2}$), *dGALT* mutant ($dGALT^{\Delta AP2}$), and double mutant ($dGALT^{\Delta AP2}$; $dGALE^{h}$). (**B**) Wg intensity in single and double mutants normalized to appropriate genetic controls. (**C**) NMJ boutons imaged with anti-HRP (green) and anti-Dally-like Protein (Dlp, red) in the same 5 genotypes. (**D**) Dlp intensity in single and double mutants normalized to genetic controls. (**E**) Representative NMJs probed with anti-HRP (red) and anti-Futsch (green) in the same 5 genotypes. (**F**) Percentage of Futsch-positive loop boutons in single and double mutants. (**G**) Higher magnification image of a microtubule loop within a single synaptic bouton probed with membrane anti-HRP (red), anti-Futsch (green) and the merged channels. Sample size: ≥10 NMJs/animals per genotype. Error bars show SEM with significance indicated as *P≤0.05, **P≤0.01 and ***P≤0.001.

trans-synaptic signalling pathway to similarly alter NMJ synaptogenesis and impair coordinated movement. We tested this hypothesis by assaying the dual outputs of the Wg pathway; 1) presynaptic Wg activation of Futsch/MAP1b remodeling of the synaptic bouton microtubule cytoskeleton (47) and 2) postsynaptic Wg activation of the Frizzled nuclear import (FNI) pathway involving cleavage of the Frizzled-2 (Fz2) receptor and trafficking of the carboxyl-terminal signalling domain (Fz2-C) to the muscle nuclei (48–50). Representative images and data summaries of these analyses are shown in Figures 6 and 7.

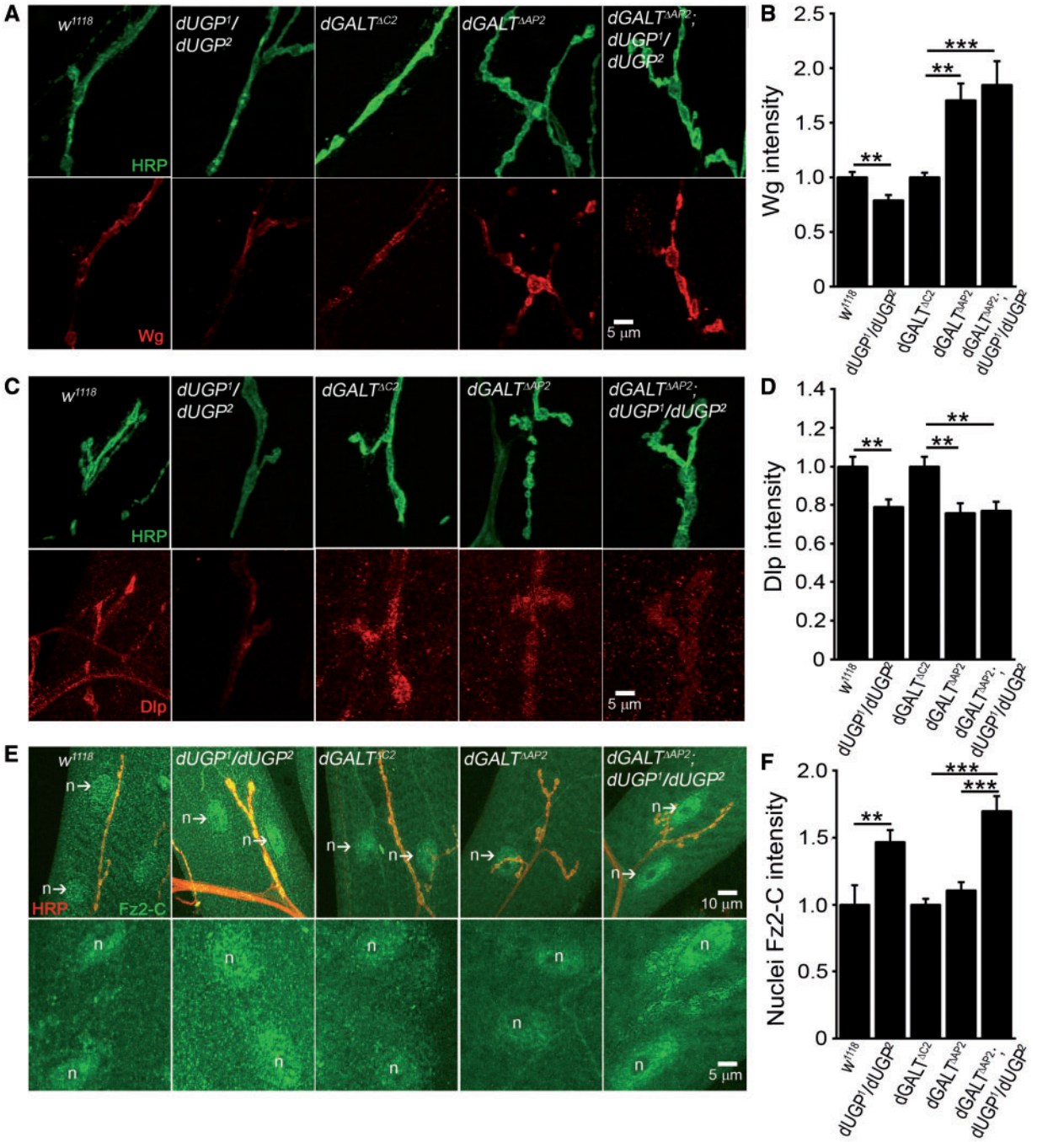

Figure 7. Postsynaptic Wnt signalling upregulated in *dUGP* and *dGALT* double mutant. (**A**) Representative NMJ boutons co-labelled with anti-HRP (green) and anti-Wg (red) in genetic control (w^{1118}), *dUGP* mutant ($dUGP^1/dUGP^2$); precise excision control ($dGALT^{\Delta C2}$), *dGALT* single ($dGALT^{\Delta AP2}$) and double ($dGALT^{\Delta AP2}$; $dUGP^1/dUGP^2$) mutants. (**B**) Quantification of Wg intensity normalized to genetic controls. (**C**) NMJ boutons imaged with anti-HRP (green) and anti-Dlp (red) in the same 5 genotypes. (**D**) Quantification of Dlp intensity in single and double mutants normalized to genetic controls. (**E**) NMJs probed with anti-HRP (red) and anti-Fz2-C (Fz2-C, green) in the same 5 genotypes. The bottom row shows nuclear Fz2-C labelling only. The "n" labels postsynaptic muscle nuclei. (**F**) Quantification of Fz2-C intensity within muscle nuclei. Sample size: ≥7 NMJs/animals per genotype. Error bars show SEM with significance indicated as $^*P \leq 0.05$, $^{**}P \leq 0.01$ and $^{***}P \leq 0.001$.

Compared to w^{1118} genetic background controls, *dGALE* mutant NMJs display a striking and immediately obvious loss of the Wg signalling ligand (Figure 6A). In quantifying Wg label intensity, $dGALE^h$ exhibits a highly significant ~50% decrease in Wg compared to matched controls ($n = 10,10$; $P = 0.0007$; Figure 6B). This contrasts sharply with *dGALT* mutants, which show the opposite ~50% increase in Wg levels compared to matched controls ($n = 31,36$; $P < 0.001$; Figure 6A,B). Perhaps additively, double mutants ($dGALE^h/dGALE^h$; $dGALT^{\Delta AP2}/dGALT^{\Delta AP2}$) show a restoration of Wg ligand levels to the wildtype condition ($n = 23$; $P < 0.001$ compared to $dGALT^{\Delta AP2}$; Figure 6A,B). In contrast, compared to genetic controls both *dGALE* and *dGALT* mutant NMJs display lower levels of the Wg co-receptor Dlp (Figure 6C). Quantification of Dlp labelling intensity shows a similar ~20% loss in $dGALE^h$ compared to controls ($n = 15,16$; $P = 0.03$) and $dGALT^{\Delta AP2}$ compared to controls ($n = 56,59$; $P < 0.05$; Figure 6D).

Double mutants were not significantly worse than the single mutants alone, but display a very significant loss of Dlp compared to matched controls ($n = 26,59$; $P < 0.01$; Figure 6D). These results show that *dGALE* strongly impacts Wg pathway components, but that *dGALE* effects on Wg ligand are different compared to *dGALT*, with a similar effect on the Wg co-receptor.

In presynaptic Fz2 receptor activation, Wg binds the receptor to drive phosphorylation of Futsch/MAP1b, which mediates NMJ growth and bouton formation via regulation of the synaptic microtubule cytoskeleton (48). To assay this pathway, *dGALE* and *dGALT* single and double mutants were co-labelled with anti-Futsch (green) compared to anti-HRP (red), with Futsch labelling quantified in synaptic boutons as absent, bundled, diffuse or looped (48) (Figure 6E). In quantifying these different categories, $dGALE^{h}$ single mutants display a significantly greater percentage of looped boutons (0.13 ± 0.03, $n = 14$) compared to w^{1118} controls (0.05 ± 0.01, $n = 15$, $P = 0.023$; Figure 6F). Similarly, $dGALT^{\Delta AP2}$ mutants show a higher level of Futsch loops (0.17 ± 0.02, $n = 28$, Figure 6G) compared to $dGALT^{\Delta C2}$ genetic background controls (0.09 ± 0.01, $n = 36$, $P < 0.001$; Figure 6F). The double mutants ($dGALE^{h}/dGALE^{h}$; $dGALT^{\Delta AP2}/dGALT^{\Delta AP2}$) exhibit greatly elevated Futsch loops in synaptic boutons (0.19 ± 0.02, $n = 24$), a highly significant increase compared to matched controls ($P < 0.001$; Figure 6F). These results show *dGALE* and *dGALT* display Futsch-driven microtubule changes predictive of the above NMJ overelaboration defects (47). In postsynaptic receptor activation, Wg binding causes Fz2-C cleavage and trafficking to muscle nuclei (49,50), which can be quantified by measuring anti-Fz2-C nuclear fluorescence intensity. For all *dGALE* and *dGALT* single and double mutants, Fz2-C accumulation in the nuclei is not significantly different from matched controls (control: 1 ± 0.05; *dGALT* single mutants: 0.96 ± 0.08; and double mutant animals: 0.90 ± 0.09). These results indicate that both *dGALE* and *dGALT* selectively impact presynaptic Wg signalling.

We next turned to testing *dUGP* roles in Wg signalling, either in the presence and absence of *dGALT* (Figure 7). Like *dGALE*, $dUGP^{1}/dUGP^{2}$ mutants exhibit significantly lower Wg ligand levels at the NMJ compared to w^{1118} controls ($n = 28,36$; $P = 0.0038$; Figure 7A,B). However, unlike *dGALE*, the double mutants ($dGALT^{\Delta AP2}/dGALT^{\Delta AP2}$; $dUGP^{1}/dUGP^{2}$) did not revert the elevated Wg ligand levels characterizing $dGALT^{\Delta AP2}$ alone ($n = 34,46$; $P < 0.01$ compared to $dGALT^{\Delta C2}$ control), but rather display a modest further increase (~15%) in Wg ligand abundance ($n = 33$, $P < 0.001$; Figure 7A,B). Like *dGALE*, *dUGP* mutants ($dUGP^{1}/dUGP^{2}$) show a ~20% decrease in the Wg co-receptor Dlp ($n = 18$) compared to w^{1118} controls ($n = 19$, $P = 0.002$; Figure 7C,D). Similar to *dGALT* nulls ($n = 28$), double mutants also display a significant Dlp depletion at the NMJ ($n = 20$), which is very significantly lower than matched controls ($n = 31$, $P < 0.01$; Figure 7D). Pre- and postsynaptic Wg signalling was next explored. In the presynaptic pathway, the number of Futsch-positive bouton loops in *dUGP* single mutants (Futsch-positive bouton loops/total number of boutons: 0.09 ± 0.02, $n = 6$) is indistinguishable from appropriate controls (Futsch-positive bouton loops/total number of boutons: 0.05 ± 0.01, $n = 15$). Our findings confirm the elevated Futsch loops that characterized the single *dGALT* mutant condition (Futsch-positive bouton loops/total number of boutons: 0.20 ± 0.02, $n = 11$, $P = 0.002$), compared to the precise excision control group (Futsch-positive bouton loops/total number of boutons: 0.08 ± 0.02, $n = 10$). This trait remains unaffected by the co-removal of *dUGP* (Futsch-positive bouton loops/total number of boutons: 0.20 ± 0.03, $n = 10$) In the postsynaptic pathway, however, nuclear Fz2-C accumulation is very significantly increased by ~50% in $dUGP^{1}/dUGP^{2}$ mutants compared to w^{1118} genetic controls ($n = 16, 7$; $P < 0.01$; Figure 7E, F). As reported above, *dGALT* nulls again show no significant difference in nuclear Fz2-C levels compared to controls ($n = 48,40$; Figure 7E,F), however the double mutants ($dGALT^{\Delta AP2}/dGALT^{\Delta AP2}$; $dUGP^{1}/dUGP^{2}$, $n = 25$) exhibit a very striking increase in Fz2-C nuclear localization compared to both controls ($P < 0.001$) and *dGALT* alone ($P < 0.001$; Figure 7E,F). These findings suggest that specifically increased activation of the postsynaptic FNI pathway underlies *dUGP* NMJ synaptogenesis and coordinated movement deficits.

Discussion

Galactosemias result from deficits in any of the three enzymes of the Leloir pathway: GALK, GALT and GALE. Through this highly conserved cascade, galactose is converted into precursors for the galactosylation of proteins and lipids (2). This mechanism is thought to be the key to disease state chronic neurological symptoms (51,52), particularly in the transferase- and epimerase-associated galactosemias. We previously discovered severe galactose glycan losses, synaptogenesis defects and changes in Wnt *trans*-synaptic signalling components at the neuromuscular synapse correlated with coordinated movement impairments in the *Drosophila GALT*-deficient galactosemia disease model (12). Since the long-term neurodevelopmental and movement symptoms reported for *GALE*-deficient galactosemia are similar (11), we set forth here to characterize a new *Drosophila GALE*-deficient neurological disease model. Unlike GALT and GALK, no human patient completely lacking GALE activity has been reported (13), consistent with the essential requirement for GALE in *Drosophila* and *C. elegans* (34,35). Thus, while most severe *GALT*-deficient patients have no detectable enzymatic activity (53), the most severe *GALE*-deficient patients reported exhibit ≥5% residual activity (54). Consistently, we report here on *dGALE* mutants with ~8% enzymatic activity, as well as targeted neuronal *dGALE* knockdown, and show both display compromised coordinated movement and NMJ synaptogenesis defects as severe as *dGALT* nulls completely lacking enzymatic activity (55).

Both *dGALT* and *dGALE* mutants show striking impairments in coordinated movement. These mutant classes both move in an overtly uncoordinated manner, and roll over slowly after being placed in an inverted position (56). This twist-and-roll response is a complex behaviour requiring the animal to contract multiple muscles on one side in a close sequence, while simultaneously relaxing contralateral muscles. Such bilateral motor control requires tight regulation of neuromuscular connectivity (12,57). Consistently, aberrant NMJ architecture is associated with the striking coordination deficits in both *dGALT* and *dGALE* mutant animals. Double *dGALE; dGALT* mutants show an additive exacerbation of the behavioural phenotypes. Since *dGALE* is downstream of *dGALT* in the pathway, one might predict that double mutant animals would behave like *dGALT* single mutants. The fact that this is not the case indicates that these enzymes must have non-overlapping functions outside of the linear Leloir pathway (58). What might be the basis of this genetic interaction? Unlike dGALT, dGALE mediates an energetically-reversible enzymatic reaction (Figure 1A). In the absence of *dGALT*, there is little UDP-galactose present, which has been suggested to shift the reversible dGALE reaction towards the formation of UDP-galactose from UDP-glucose (30). Loss of dGALE activity would not allow for such a responsive shift and would account for the worsening of the *dGALT* coordinated movement phenotypes reported here.

UDP-glucose pyrophosphorylase represents an alternate GALT-independent route for galactose metabolism (9). UGP catalyzes the formation of UDP-glucose from glucose-1-phosphate and UTP, but can also catalyze the formation of UDP-galactose from galactose-1-P and UTP (6,9). This second function is proposed to occur particularly with high levels of galactose-1-P, such as occurs in *GALT*-deficient galactosemia (11). Importantly, overexpression of human *UGP2 (hUGP2)*, the ortholog for *dUGP*, in the yeast system has shown the ability to rescue galactose-dependent survival of *GALT*-deficient strains (59). It has therefore been hypothesized that UGP2 upregulation could also protect against long-term neurological complications in *GALT*-deficient galactosemia. Consistently, our studies reveal that *dUGP* deficiency is indeed a strong negative modulator of neurobehavioural outcomes. Null *dGALT* coordinated movement deficits are exacerbated in *dGALT*; *dUGP* double mutant combinations. Similar to dGALE, dUGP mediates a reversible enzymatic reaction (Figure 1A), and can alternately use galactose as the enzymatic substrate (6,9). Under *dGALT* null conditions where there are increasing amounts of galactose-1-P, the dUGP reaction would shift towards the formation of UDP-galactose from galactose-1-P, in order to restore the UDP-sugar balance for proper glycosylation. Based on this interaction, co-removal of *dUGP* would be predicted to aggravate coordinated movement deficits in the double mutants, as reported here.

NMJ synaptogenesis is regulated by distinct mechanisms controlling axonal branching and synaptic bouton maturation (60,61). Indeed, while new bouton formation is plastic, activity-dependent and occurs at variable rates throughout postembryonic development, the number of synaptic branches is established early and remains relatively stable thereafter (60,61). Like *dGALT*, *dGALE* mutants strongly restrict synaptic bouton development but, unlike *dGALT*, do not affect synaptic branching. Loss of *dGALE* augments only the number of synaptic boutons, whereas double *dGALE; dGALT* mutant animals display an increase in both branching and supernumerary bouton formation. Likewise, loss of *dUGP* significantly increases new synaptic bouton formation in both heterozygous and transheterozygous conditions, demonstrating the need for >50% dUGP activity for proper NMJ synaptic morphogenesis. Like *dGALE*, *dUGP* mutants have only a minimal impact on NMJ branching, although co-removal of *dGALT* augments the axonal branching defect in double mutant conditions. These findings show a clear need for *dGALT, dGALE* and *dUGP* in limiting synaptic bouton development, whereas *dGALT* and to a lesser extent *dUGP* are also required earlier to establish a proper synaptic branching architecture. This *dUGP* involvement is not surprising, since it is the only enzyme in *Drosophila* capable of synthesizing UDP-glucose, which is well-known to have a central role in anabolic and catabolic pathways regulating cell growth and development (38–40).

We have previously shown that dGALT activity did not significantly alter functional differentiation driving neurotransmission strength at the NMJ, but rather appears to specifically modulate synaptic architecture (12). This is possible since NMJ structure and function are well established to be independently regulated, and coordinated movement defects can occur with NMJ structural defects in the absence of overt synaptic transmission defects (56). The result is surprising, however, since N-glycans have been causally implicated in both *Drosophila* NMJ structural and functional synaptogenesis (21,22). Consistent with the essential role of dGALE in the biosynthesis of glycoconjugates (62–64), we find here that dGALE is a strong determinant of neurotransmission strength, with significantly elevated synaptic function under conditions of reduced dGALE activity. Moreover, neurotransmission is further elevated with co-removal of dGALT, showing a significant genetic interaction upstream of synaptic function. However, like dGALT, viable levels of dUGP loss do not have a similar impact on neurotransmission strength. There is no significant change in NMJ function either in the single *dUGP* mutant condition, or with co-removal of dGALT. Unlike dGALE, dUGP is not at the crossroads of UDP sugar balance and this perhaps explains the differential requirement of the two enzymes in synaptic functional differentiation.

NMJ synaptogenesis is highly dependent on extracellular glycan mechanisms (5). Indeed, we previously demonstrated *dGALT* null NMJ overelaboration is driven by a striking depletion of galactosyl, N-acetylgalactosamine and fucosylated HRP moieties within the synaptomatrix (12). However, only loss of N-acetylgalactosamine is rescued by *hGALT* expression, and is reduced in wildtype animals after galactose overfeeding, suggesting this is the primary causative synaptic glycan change (12). Similar to *dGALT*, *C. elegans GALE* loss-of-function causes strong reduction of UDP-galNAc levels, accompanied by developmental defects associated with UDP-galNAc deficits (35). Importantly, GALE is primarily responsible for UDP-galNAc biosynthesis, since UDP-galNAc cannot be synthesized by GALE-independent pathways (Figure 1A). Consistently, our *Drosophila GALE*-deficient galactosemia model exhibits a dramatic loss of GalNAc in the NMJ synaptomatrix. Furthermore, concomitant removal of *dGALE* and *dGALT* strikingly exacerbates GalNAc losses compared to the single *dGALT* null condition. *dUGP*-deficient animals also manifest loss of GalNAc in the NMJ synaptomatrix. Moreover, both *dGALE* and *dUGP* mutants similarly display synaptic loss of HRP epitope, revealing bifucosylated N-glycans. This apparent cross-talk between Leloir and GDP-Fucose production pathways is intriguing, especially in the absence of a Fucose salvage route in *Drosophila*. It would be interesting to determine how altered nucleotide sugar metabolism affects protein glycosylation in addition to processing. In eukaryotes, fucosylation occurs primarily in the Golgi, and recent evidence suggests a close connection between UDP-sugar balance and Golgi N-glycan branching (65), which may explain these findings. Furthermore, recent studies from our lab (12,22) provide evidence that HRP glycan loss is accompanied by increased synaptic growth, similar to what we report here for both *dGALE* and *dUGP* mutants.

NMJ synaptogenesis is modulated by *trans*-synaptic signalling that occurs via secreted glycoprotein ligands traversing the highly-glycosylated synaptomatrix (5,66,67). In particular, the founding Wnt Wingless (Wg) signalling ligand is a potent driver of synaptic development (50,68). Wg is secreted from presynaptic neuron and glia to bind Fz2 receptors on both neuron and postsynaptic muscle via interaction with the Wg co-receptor HSPG Dlp, a well-known regulator of Wg extracellular distribution and signalling (21,68,69). Postsynaptic Wg activates the Frizzled nuclear import (FNI) pathway, in which Fz2 is endocytosed followed by the cleavage and nuclear trafficking of the C-terminus (Fz2-C) to regulate synaptogenesis (50). Presynaptic Wg activates Futsch/MAP1B phosphorylation and binding to the synaptic microtubule cytoskeleton, driving the budding of new synaptic boutons and NMJ expansion (47,48) Null *dGALT* NMJs exhibit elevated Wg and reduced Dlp^{12}, but the impact on Wg signal transduction was not previously investigated. We discover here that postsynaptic FNI signalling is not affected in the *dGALT*-deficient galactosemia model, but rather there is a strong upregulation of presynaptic Futsch signalling, consistent with the observed elevated synaptic bouton formation (47). Likewise,

the new *dGALE*-deficient galactosemia model shows specific hyper-activation of presynaptic Futsch-mediated microtubule rearrangements modulating NMJ morphogenesis. Thus, both galactosemia disease models similarly activate the presynaptic Wnt pathway.

In contrast to *dGALT* and *dGALE* requirements, *dUGP* mutants specifically activate the postsynaptic FNI pathway. Presynaptic Wg activation requires the inhibition of the Glycogen Synthase Kinase 3β (GSK3β) homolog Shaggy (Sgg) (70), a protein kinase with the ability to phosphorylate glycogen synthase. Previous experiments have demonstrated that *UGP* loss is associated with increased phosphorylation of glycogen synthase and subsequent reduction of its catalytic activity (38). This predicts that GSK3β is hyper-activated in *dUGP* mutants, which would prevent Wg activation of the presynaptic pathway. As we have shown many times previously (21–23), predicting the directionality of Wg signalling changes based on Wg ligand, Fz2 receptor levels and Dlp co-receptor is profoundly difficult owing to the interplay between the 3 players, as described in the 'Exchange Factor Mechanism'(21,23,71). Wg may be actively signalling or sequestered extracellularly in a non-signalling state, and Dlp plays both positive and negative roles in signalling, dependent on the relative abundance of Wg and Fz2 (71), as well as other factors. In the galactosemia disease models, extracellular Wg abundance is oppositely misregulated in *dGALT* vs. *dGALE* mutants, although the presynaptic signalling activation is similar. Likewise, *dGALT* and *dUGP* mutants exhibit an opposite effect on Wg ligand levels, but only *dUGP* mutants show a significant activation of the postsynaptic FNI pathway. We hypothesize that the fundamental defect in Leloir pathway mutants is the altered levels of the Wg co-receptor HSPG Dlp, which are low in both single and double mutant combinations. Previous studies have associated reduced Dlp levels to locally increased extracellular Wg levels (69,72), as is the case for *dGALT* mutants, and activation of Wg signalling, similar to what we report here. The direction of Wg activation, pre- or postsynaptic, appears different in *dGALT*, *dGALE* and *dUGP* mutants due to additional factors that we have yet to resolve. The identity and role of Wnt pathway ligand/receptor/coreceptor changes, and directional signalling defects at the NMJ, will be the focus of our future studies.

In conclusion, the results presented here are the first to reveal coordinated movement deficits, NMJ structure and functional defects, NMJ glycosylation losses and differential Wnt *trans*-synaptic signalling dysfunction under conditions of *GALE*-deficient galactosemia and *UGP2* deficiency. Unlike *GALT*-deficient galactosemia, both *GALE* and *UGP2* are indispensable for viability, and substantial residual enzymatic activities are required for survival, but nevertheless partial loss-of-function manifests severe neurobehavioural defects due to a neuronal requirement. *GALE*-deficient galactosemia shares with classic galactosemia numerous pathogenic factors underlying the long-term neurological impairments characterized by coordinated movement disabilities. Our results suggest that changes in Wnt signalling and Futsch/MAP1B microtubule cytoskeletal organization underlie neuromuscular synapse development defects and impaired coordinated movement in both disease states. Our results also reveal UGP2 activity and GalNAc glycosylation roles in neuromuscular synaptogenesis, raising the intriguing possibilities that targeted UGP2 strategies and/or UDP-galNAc supplementation might relieve neurological complications in the galactosemia disease states, as previously suggested (59,62).

Materials and Methods

Drosophila genetics

Figure 1A shows in parallel the enzymatic steps of the glucose and galactose metabolic pathways, listing the names and *Drosophila* CG numbers of all the genes targeted in this study, as well as the biochemical functions of the encoded proteins. All stocks were obtained from the Bloomington *Drosophila* Stock Center and Vienna *Drosophila* Resource Center, and reared at 25°C under low-density rearing conditions on standard molasses-based food. We used two *dGALT* excision alleles generated by mobilizing a P-element insertion in the 5'-untranslated region of *CG9232* (*KG00049*); $dGALT^{\Delta C2}$ (precise excision control) and $dGALT^{\Delta AP2}$ (null deficiency), with measured normal and undetectable enzymatic activity, respectively (55). A *dGALE* (*CG12030*) allele, $dGALE^{h}$, was generated by mobilizing P-element insertion *P{EPgy2}CG12030*^{EY22205} with *H{PDelta2-3}HoP8,y*^{1}*w*;Dr/TM3,Sb* (34). Activity assays show $dGALE^{h}$ is a strong hypomorphic allele (measured ~8% enzymatic activity), with unaltered *dGALK and dGALT* activities (34). The UAS-*dGALE-RNAi* line w^{1118}*; P{GD7464}v47408* was compared to *Gal4* driver alone controls. UH1-Gal4 driven UAS-*dGALE-RNAi* results in 100% lethality, consistent with the essential requirement for the gene (33). We used two *dUGP* stocks; w^{1118}*; PBac{WH}UGP*^{f03515}*/TM6B, Tb*^{1} ($dUGP^{1}$) and w^{1118}*; P{XP}UGP*^{d07256}*/TM6B, Tb*^{1} ($dUGP^{2}$) generated by P-element insertion (42); and UAS-*dUGP-RNAi* line *P{GD11288}v21832* for tissue-targeted experiments. Pan-neuronal *elav-Gal4* and muscle *24B-Gal4* driver were used for tissue-specific studies, compared to driver alone controls. *dGALE* and *dUGP* hypomorphic alleles were used to create double mutant stocks with $dGALT^{\Delta AP2}$. w^{1118} was used as the genetic background control for *dGALE* and *dUGP*, and precise excision controls $dGALT^{\Delta C2}$ were used in double mutant combinations of these alleles.

Behavioural assays

Movement assays were performed as previously described in isolated wandering third-instar (wL3) male larvae (56). Larvae were placed individually on a fresh, room temperature (RT) 1% agar plate and allowed to move freely for ~2 min before the assay. Using forceps, the larva was rolled to an inverted position as defined by the upright ventral midline. Once released, a timer recorded the amount of time the larva took to completely right itself as defined by the upright dorsal midline (56). Three consecutive time measurements were recorded for each larva and then averaged to produce one data point. The maximum amount of time allowed for a given animal to rollover was 5 minutes. Behavioural experiments were done on ≥15 individual animals for each genotype. Data were analyzed by student's t-test for pairwise comparisons, and ANOVA tests for all data sets of ≥3 comparisons.

Immunocytochemical imaging

Wandering L3 larvae were used for all immunocytochemistry imaging as previously described (21,73). Reagents were purchased from Sigma-Aldrich unless otherwise specified. Larvae were dissected in physiological saline (128mM NaCl, 2mM KCl, 4mM $MgCl_2$, 0.2mM $CaCl_2$, 70mM sucrose, 5mM trehalose, 5mM HEPES), fixed in 4% paraformaldehyde for 10 minutes at RT, and then either processed with PBTX (PBS + 1% BSA + 0.2% Triton X-100) detergent, for cell permeabilized studies, or detergent-free (PBS with 1% BSA or without BSA when using lectins) conditions, for

non-permeabilized studies. Primary antibodies included: Alexa Fluor-488 goat anti-horseradish peroxidase (HRP, 1:200, Jackson Labs); Cy3-conjugated goat anti-HRP (1:200, Jackson Labs); mouse anti-Fasciclin II (FasII, 1:10, Developmental Studies Hybridoma Bank (DSHB), University of Iowa); mouse anti-Discs Large (DLG, 1:250; DSHB); mouse anti-Wingless (Wg, 1:2; DSHB); mouse anti-Dally-like Protein (Dlp, 1:4; DSHB); rabbit anti-dFz-C (1:500) (75); mouse anti-Futsch (1:100; DSHB). Secondary antibodies included: Alexa Fluor-488-conjugated goat anti-mouse IgG (1:200, Invitrogen-Molecular Probes) and Alexa Fluor-488-conjugated goat anti-rabbit IgG (1:250, Invitrogen-Molecular Probes). *Wisteria floribunda* (WFA-Fitc, 1:250, Vector Labs) was used as fluorophore-conjugated lectin to label N-acetyl galactosamine residues (12). Primary antibodies and lectins were incubated at 4 °C overnight; secondary antibodies were incubated at RT for 2 hrs. Dissections were mounted on slides in Fluoromount G (Electron Microscopy Sciences).

All mutant and control larvae were dissected, labelled and imaged completely in parallel. Z-stacks were taken with a Zeiss LSM 510 META laser-scanning confocal, using either 40x or 63x Plan Apo oil-immersion objectives. Optical sections were taken starting immediately above and ending immediately below the NMJ. The stacks were projected on the Z-axis, with NMJ signals highlighted and the average intensity for each NMJ recorded. Intensities were quantified using *ImageJ* software. For structural analyses, preparations were double-labelled with anti-HRP and anti-DLG, with counts made at muscle 4 in segments A2/3 on both right and left sides. Structural data from hemisegments were averaged for each animal to produce one data point. For quantification, a bouton was defined as an axon varicosity $>1\mu m$ in minimum diameter, and >2 boutons on an axon defined a NMJ branch. For quantification of Wg *trans*-synaptic signalling components (i.e. Wg ligand, HSPG Dlp, Fz2-C and Futsch), each NMJ was treated as an independent replicate. For Futsch labelling, NIH *ImageJ* was used to count bouton numbers, with high magnification imaging used to classify all boutons as empty (no Futsch labelling), diffuse (Futsch-positive, unorganized), bundled (Futsch-positive bundle) and looped (Futsch-positive loop) (48).

Electrophysiology

Two-electrode voltage-clamp (TEVC) electrophysiology was performed as previously described (74). Briefly, wL3 were secured with 3M Vetbond tissue adhesive (World Precision Instruments) to sylgard-coated glass coverslips, cut longitudinally along the dorsal midline, internal organs removed, and the larval cuticle glued down laterally to allow access to the neuromusculature. Peripheral nerves were then cut at the base of the ventral nerve cord (VNC). Dissections and recordings were performed at 18 °C in saline solution consisting of 128mM NaCl, 2mM KCl, 4mM $MgCl_2$, 1.0mM $CaCl_2$, 70mM sucrose, 5mM trehalose and 5mM HEPES, with pH adjusted to 7.1 using NaOH. Preparations were imaged using a Zeiss Axioskop microscope with 40X water immersion objective. Muscle 6 in abdominal segments 2/3 was impaled with two microelectrodes of $\sim$15 MΩ resistance filled with 3M KCl. The muscle was clamped at -60 mV using an Axoclamp-2B amplifier. A fire-polished glass suction electrode containing saline was used for evoked nerve stimulation of the severed motor nerve with a 0.5 ms suprathreshold stimuli at 0.2 Hz from a Grass S88 stimulator (74). Excitatory junctional current (EJC) records were filtered at 2 kHz. To quantify EJC amplitudes, 10 consecutive traces were averaged and the peak of the averaged trace recorded. Clampex software was used for all data acquisition and Clampfit software was used for all data analyses.

Statistical Analyses

All behavioural and NMJ structural data were averaged per genotype and each replicate value was calculated as the fold-change relative to the average value of the appropriate control. For signal intensity and structural data, control and mutant animals were always dissected, labelled and imaged in parallel. Intensity was calculated as the fold-change relative to the average control value recorded in the same experiment. The proportion of boutons displaying Futsch-positive loops was calculated relative to the total number of boutons at each NMJ. Unpaired t-tests (pairwise comparisons) or Mann-Whitney tests ($\geq$3 comparisons) were used to compare differences between mutants and controls as indicated in figure legends. The criterion for statistical significance was $P \leq 0.05$, with higher levels of significance classified as $P \leq 0.01$, $P \leq 0.001$ and $P \leq 0.0001$. All statistical analyses were performed using GraphPad InStat version 3.0 (GraphPad Software, San Diego California, USA).

Acknowledgements

This work was solely supported by National Institutes of Health grant MH096832 to K.B. We are grateful to Vivian Budnik (University of Massachusetts Medical School, Worchester MA) for antibody reagents. We also particularly thank the Developmental Studies Hybridoma Bank at the University of Iowa for essential antibodies, and the *Drosophila* Bloomington Stock Center at Indiana University and Vienna *Drosophila* Resource Center for essential genetic lines.

Conflict of Interest statement. None declared.

Funding

This work was fully funded by NIH grant R01 MH096832 to K.B.

References

1. Bosch, A.M. (2006) Classical galactosaemia revisited. *J. Inherit. Metab. Dis.*, **29**, 516–525.
2. Holden, H.M., Rayment, I. and Thoden, J.B. (2003) Structure and function of enzymes of the Leloir pathway for galactose metabolism. *J. Biol. Chem.*, **278**, 43885–43888.
3. Freeze, H.H. and Elbein, A.D. (2009). Glycosylation Precursors. *Essentials of Glycobiology*, 2nd edition, Cold Spring Harbor Laboratory Press, Cold Spring Harbor, NY.
4. Prydz, K. and Dalen, K.T. (2000) Synthesis and sorting of proteoglycans. *J. Cell Sci.*, **113**, 193–205.
5. Dani, N. and Broadie, K. (2012) Glycosylated synaptomatrix regulation of trans-synaptic signaling. *Dev. Neurobiol.*, **72**, 2–21.
6. Turnquist, R.L., Gillett, T.A. and Hansen, R.G. (1974) Uridine diphosphate glucose pyrophosphorylase. Crystallization and properties of the enzyme from rabbit liver and species comparisons. *J. Biol. Chem.*, **249**, 7695–7700.
7. Geisler, M., Wilczynska, M., Karpinski, S. and Kleczkowski, L.A. (2004) Toward a blueprint for UDP-glucose pyrophosphrylase structure/function properties: homology-modeling analyses. *Plant Mol./Biol.*, **56**, 783–794.
8. Yu, Q. and Zheng, X. (2012) The crystal structure of human UDP-glucose pyrophosphorylase reveals a latch effect that influences enzymatic activity. *Biochem. J.*, **442**, 283–2913.
9. Isselbacher, K.J. (1958) A mammalian uridinediphosphate galactose pyrophosphorylase. *J. Biol. Chem.*, **232**, 429–444.

10. CDC Grand Rounds (2012): Newborn Screening and Improved Outcomes. *Morbidity and Mortality Weekly Report (MMWR)*. Available: http://www.cdc.gov/mmwr/preview/mmwrhtml/mm6121a2.htm.
11. Fridovich-Keil, J.L. (2006) Galactosemia: the good, the bad, and the unknown. *J. Cell Physiol.*, **209**, 701–705.
12. Jumbo-Lucioni, P., Parkinson, W. and Broadie, K. (2014) Overelaborated synaptic architecture and reduced synaptomatrix glycosylation in a *Drosophila* classic galactosemia disease model. *Dis. Model Mech.*, **7**, 1365–1378.
13. Fridovich-Keil, J., Bean, L., He, M. and Schroer, R. (2011). *Epimerase Deficiency Galactosemia. GeneReviews® [Internet]*. Seattle (WA): University of Washington, Seattle; 1993-2015. Available from: http://www.ncbi.nlm.nih.gov/books/NBK51671/.
14. Hennermann, J.B., Schadewaldt, P., Vetter, B., Shin, Y.S., Monch, E. and Klein, J. (2011) Features and outcome of galactokinase deficiency in children diagnosed by newborn screening. *J. Inherit. Metab. Dis.*, **34**, 399–407.
15. Janzen, N., Illsinger, S., Meyer, U., Shin, Y.S., Sander, J., Lucke, T. and Das, A.M. (2011) Early cataract formation due to galactokinase deficiency: impact of newborn screening. *Arch. Med. Res.*, **42**, 608–612.
16. Timson, D.J. (2015) The molecular basis of galactosemia - Past, present and future. *Gene*, doi: 10.106/j.gene.2015.06.077.
17. Holton, J.B., Gillett, M.G., MacFaul, R. and Young, R. (1981) Galactosaemia: a new severe variant due to uridine diphosphate galactose-4-epimerase deficiency. *Arch. Dis. Child.*, **56**, 885–887.
18. Haberland, C., Perou, M., Brunngraber, E.G. and Hof, H. (1971) The neuropathology of galactosemia. A histopathological and biochemical study. *J. Neuropathol. Exp. Neurol.*, **30**, 431–447.
19. Petry, K., Greinix, H.T., Nudelman, E., Eisen, H., Hakomori, S., Levy, H.L. and Reichardt, J.K.V. (1991) Characterization of a novel biochemical abnormality in galactosemia: deficiency of glycolipids containing galactose or N-acetylgalactosamine and accumulation of precursors in brain and lymphocytes. *Biochem. Med. Metab. Biol.*, **46**, 93–104.
20. Charlwood, J., Clayton, P., Keir, G., Mian, N. and Winchester, B. (1998) Defective galactosylation of serum transferrin in galactosemia. *Glycobiology*, **8**, 351–357.
21. Dani, N., Nahm, M., Lee, S. and Broadie, K. (2012) A targeted glycan-related gene screen reveals heparan sulfate proteoglycan sulfation regulates WNT and BMP trans-synaptic signaling. *PLoS Genet.*, **8**, e1003031.
22. Parkinson, W., Dear, M.L., Rushton, E. and Broadie, K. (2013) N-glycosylation requirements in neuromuscular synaptogenesis. *Development*, **140**, 4970–4981.
23. Friedman, S.H., Dani, N., Rushton, E. and Broadie, K. (2013) Fragile X mental retardation protein regulates trans-synaptic signaling in *Drosophila*. *Dis. Model Mech.*, **6**, 1400–1413.
24. Waggoner, D.D., Buist, N.R. and Donnell, G.N. (1990) Long-term prognosis in galactosaemia: results of a survey of 350 cases. *J. Inherit. Metab. Dis.*, **13**, 802–818.
25. Schweitzer, S., Shin, Y., Jakobs, C. and Brodehl, J. (1993) Long-term outcome in 134 patients with galactosaemia. *Eur. J. Pediatr.*, **152**, 36–43.
26. Kaufman, F.R., McBride-Chang, C., Manis, F.R., Wolff, J.A. and Nelson, M.D. (1995) Cognitive functioning, neurologic status and brain imaging in classical galactosemia. *Eur. J. Pediatr.*, **154**, S2–S5.
27. Hughes, J., Ryan, S., Lambert, D., Geoghegan, O., Clark, A., Rogers, Y., Hendroff, U., Monaravi, A., Twomey, E. and Treacy, E.P. (2009) Outcomes of siblings with classical galactosemia. *J. Pediatr.*, **154**, 721–726.
28. Rubio-Agusti, I., Carecchio, M., Bhatia, K.P., Kojovic, M., Parees, I., Chandrashekar, H.S., Footitt, E.J., Burke, D., Edwards, M.J., Lachmann, R.H. and Murphy, E. (2013) Movement disorders in adult patients with classical galactosemia. *Mov. Disord.*, **28**, 804–810.
29. Szklarczyk, D., Franceschini, A., Wyder, S., Forslund, K., Heller, D., Huerta-Cepas, J., Simonovic, M., Roth, A., Santos, A., TsafouK, P., *et al.* (2015) STRING v10: protein-protein interaction networks, integrated over the tree of life. *Nucleic Acids Res.*, **43**, D447–D452.
30. Prodan-Zitnik, I., Karas-Kuzelicki, N. and Lukac-Bajalo, J. (2009) Positive correlation between galactose-1-phosphate uridyltransferase (GALT) and UDP-galactose-4'-epimerase (GALE) activities. *Clin. Biochem.*, **42**, 1561–1564.
31. Walter, J.H., Roberts, R.E., Besley, G.T., Wraith, J.E., Cleary, M.A., Holton, J.B. and MacFaul, R. (1999) Generalised uridine diphosphate galactose-4-epimerase deficiency. *Arch. Dis. Child.*, **80**, 374–376.
32. Alano, A., Almashanu, S., Chinsky, J.M., Costeas, P., Blitzer, M.G., Wulfsberg, E.A. and Cowan, T.M. (1998) Molecular characterization of a unique patient with epimerase-deficiency galactosaemia. *J. Inherit. Metab. Dis.*, **21**, 341–350.
33. Daenzer, J.M., Sanders, R.D., Hang, D. and Fridovich-Keil, J.L. (2012) UDP-galactose 4'-epimerase activities toward UDP-Gal and UDP-GalNAc play different roles in the development of *Drosophila melanogaster*. *PLoS Genet.*, **8**, e1002721.
34. Sanders, R.D., Sefton, J.M., Moberg, K.H. and Fridovich-Keil, J.L. (2010) UDP-galactose 4' epimerase (GALE) is essential for development of *Drosophila melanogaster*. *Dis. Model Mech.*, **3**, 628–638.
35. Brokate-Llanos, A.M., Monje, J.M., Murdoch Pdel, S. and Munoz, M.J. (2014) Developmental defects in a *Caenorhabditis elegans* model for type III galactosemia. *Genetics.*, **198**, 1559–1569.
36. Xia, R., Liu, Y., Yang, L., Gal, J., Zhu, H. and Jia, J. (2012) Motor neuron apoptosis and neuromuscular junction perturbation are prominent features in a *Drosophila* model of Fus-mediated ALS. *Mol. Neurodegener.*, **7**, 10.
37. Courchesne, S.L., Pazyra-Murphy, M.F., Lee, D.J. and Segal, R.A. (2011) Neuromuscular junction defects in mice with mutation of dynein heavy chain 1. *PLoS One*, **6**, e16753.
38. Higuita, J.C., Alape-Giron, A., Thelestam, M. and Katz, A. (2003) A point mutation in the UDP-glucose pyrophosphorylase gene results in decreases of UDP-glucose and inactivation of glycogen synthase. *Biochem. J.*, **370**, 995–1001.
39. Flores-Diaz, M., Alape-Giron, A., Persson, B., Pollesello, P., Moos, M., von Eichel-Streiber, C., Thelestam, M. and Florin, I. (1997) Cellular UDP-glucose deficiency caused by a single point mutation in the UDP-glucose pyrophosphorylase gene. *J. Biol. Chem.*, **272**, 23784–23791.
40. Flores-Diaz, M., Alape-Giron, A., Titball, R.W., Moos, M., Guillouard, I., Cole, S., Howells, A.M., von Eichel-Streiber, C., Florin, I. and Thelestam, M. (1998) UDP-glucose deficiency causes hypersensitivity to the cytotoxic effect of Clostridium perfringens phospholipase C. *J. Biol. Chem.*, **273**, 24433–24438.
41. Daran, J.M., Bell, W. and Francois, J. (1997) Physiological and morphological effects of genetic alterations leading to a reduced synthesis of UDP-glucose in *Saccharomyces cerevisiae*. *FEMS Microbiol. Lett.*, **153**, 89–96.

42. Bellen, H.J., Levis, R.W., Liao, G., He, Y., Carlson, J.W., Tsang, G., Evans-Holm, M., Hiesinger, P.R., Schulze, K.L., Rubin, G.M., *et al*. (2004) The BDGP gene disruption project: single transposon insertions associated with 40% of *Drosophila* genes. *Genetics*, **167**, 761–781.
43. Hacker, U., Lin, X. and Perrimon, N. (1997) The *Drosophila sugarless* gene modulates Wingless signaling and encodes an enzyme involved in polysaccharide biosynthesis. *Development*, **124**, 3565–3573.
44. Sturiale, L., Barone, R., Fiumara, A., Perez, M., Zaffanello, M., Sorge, G., Pavone, L., Tortorelli, S., O'Brien, J.F., Jaeken, J. and Garozzo, D. (2005) Hypoglycosylation with increased fucosylation and branching of serum transferrin N-glycans in untreated galactosemia. *Glycobiology*, **15**, 1268–1276.
45. Dennis, J.W., Nabi, I.R. and Demetriou, M. (2009) Metabolism, cell surface organization, and disease. *Cell*, **139**, 1229–1241.
46. Tanaka, K., Kitagawa, Y. and Kadowaki, T. (2002) *Drosophila* segment polarity gene product porcupine stimulates the posttranslational N-glycosylation of wingless in the endoplasmic reticulum. *J. Biol. Chem.*, **277**, 12816–12823.
47. Roos, J., Hummel, T., Ng, N., Klambt, C. and Davis, G.W. (2000) *Drosophila Futsch* regulates synaptic microtubule organization and is necessary for synaptic growth. *Neuron*, **26**, 371–382.
48. Packard, M., Koo, E.S., Gorczyca, M., Sharpe, J., Cumberledge, S. and Budnik, V. (2002) The *Drosophila* Wnt, wingless, provides an essential signal for pre- and postsynaptic differentiation. *Cell*, **111**, 319–330.
49. Stamatakou, E. and Salinas, P.C. (2014) Postsynaptic assembly: a role for Wnt signaling. *Dev. Neurobiol.*, **74**, 818–827.
50. Koles, K. and Budnik, V. (2012) Wnt signaling in neuromuscular junction development. *Cold Spring Harb. Perspect Biol.*, **4**, pii: a008045.
51. Coss, K.P., Hawkes, C.P., Adamczyk, B., Stockmann, H., Crushell, E., Saldova, R., Knerr, I., Rubio-Gozalbo, M.E., Monaravi, A.A., Rudd, P.M. and Treacy, E.P. (2014) N-glycan abnormalities in children with galactosemia. *J. Proteome Res.*, **13**, 385–394.
52. Freeze, H.H., Eklund, E.A., Ng, B.G. and Patterson, M.C. Neurology of inherited glycosylation disorders. *Lancet Neurol.*, **11**, 453–466.
53. Holton, J.B., Walter, J.H. and Tyfield, L.A. (2000). *Metabolic and Molecular Bases of Inherited Disease*, Eighth ed., McGraw Hill, 1553–1587.
54. Wohlers, T.M. and Fridovich-Keil, J.L. (2000) Studies of the V94M-substituted human UDPgalactose-4-epimerase enzyme associated with generalized epimerase-deficiency galactosaemia. *J. Inherit. Metab. Dis.*, **23**, 713–729.
55. Kushner, R.F., Ryan, E.L., Sefton, J.M., Sanders, R.D., Lucioni, P.J., Moberg, K.H. and Fridovich-Keil, J.L. (2010) A *Drosophila melanogaster* model of classic galactosemia. *Dis. Model Mech.*, **3**, 618–627.
56. Bodily, K.D., Morrison, C.M., Renden, R.B. and Broadie, K. (2001) A novel member of the Ig superfamily, turtle, is a CNS-specific protein required for coordinated motor control. *J. Neurosci.*, **21**, 3113–3125.
57. Landmesser, L.T. (2001) The acquisition of motoneuron subtype identity and motor circuit formation. *Int. J. Dev. Neurosci.*, **19**, 175–182.
58. Frey, P.A. (1996) The Leloir pathway: a mechanistic imperative for three enzymes to change the stereochemical configuration of a single carbon in galactose. *FASEB J.*, **10**, 461–470.
59. Lai, K. and Elsas, L.J. (2000) Overexpression of human *UDP-glucose pyrophosphorylase* rescues *galactose-1-phosphate uridyltransferase*-deficient yeast. *Biochem. Biophys. Res. Commun.*, **271**, 392–400.
60. Zito, K., Parnas, D., Fetter, R.D., Isacoff, E.Y. and Goodman, C.S. (1999) Watching a synapse grow: noninvasive confocal imaging of synaptic growth in *Drosophila*. *Neuron*, **22**, 719–729.
61. Miller, D.L., Ballard, S.L. and Ganetzky, B. (2012) Analysis of synaptic growth and function in *Drosophila* with an extended larval stage. *J. Neurosci.*, **32**, 13776–13786.
62. Kingsley, D.M., Kozarsky, K.F., Hobbie, L. and Krieger, M. (1986) Reversible defects in O-linked glycosylation and LDL receptor expression in a UDP-Gal/UDP-GalNAc 4-epimerase deficient mutant. *Cell.*, **44**, 749–759.
63. Schulz, J., Ross, K., Malmstrom, K., Krieger, M. and Fridovich-Keil, J. (2005) Mediators of galactose sensitivity in UDP-galactose 4′-epimerase-impaired mammalian cells. *J. Biol. Chem.*, **280**, 13493–13502.
64. Kalckar, H.M. (1965) Galactose metabolism and cell "sociology". *Science*, **150**, 305–313.
65. Ryczko, M., Pawling, J., Chen, R., Abdel Rahman, A.M., Yau, K., Copeland, J.K., Zhang, C., Surendra, A., Guttman, D.S., Figeys, D. and Dennis, J.W. (2016) Metabolic Reprogramming by Hexosamine Biosynthetic and Golgi N-Glycan Branching Pathways. *Scientific Reports*, **6**, 23043.
66. Collins, C.A. and DiAntonio, A. (2007) Synaptic development: insights from *Drosophila*. *Curr. Opin. Neurobiol.*, **17**, 35–42.
67. Miech, C., Pauer, H.U., He, X. and Schwarz, T.L. (2008) Presynaptic local signaling by a canonical wingless pathway regulates development of the *Drosophila* neuromuscular junction. *J. Neurosci.*, **28**, 10875–10884.
68. Han, C., Yan, D., Belenkaya, T.Y. and Lin, X. (2005) *Drosophila* glypicans Dally and Dally-like shape the extracellular Wingless morphogen gradient in the wing disc. *Development.*, **132**, 667–679.
69. Kirkpatrick, C.A., Dimitroff, B.D., Rawson, J.M. and Selleck, S.B. (2004) Spatial regulation of Wingless morphogen distribution and signaling by Dally-like protein. *Dev. Cell.*, **7**, 513–523.
70. Franco, B., Bogdanik, L., Bobinnec, Y., Debec, A., Bockaert, J., Parmentier, M.L. and Grau, Y. (2004) Shaggy, the homolog of glycogen synthase kinase 3, controls neuromuscular junction growth in *Drosophila*. *J. Neurosci.*, **24**, 6573–6577.
71. Yan, D., Wu, Y., Feng, Y., Lin, S.C. and Lin, X. (2009) The core protein of glypican Dally-like determines its biphasic activity in wingless morphogen signaling. *Dev. Cell.*, **17**, 470–481.
72. Kreuger, J., Perez, L., Giraldez, A.J. and Cohen, S.M. (2004) Opposing activities of Dally-like glypican at high and low levels of Wingless morphogen activity. *Dev. Cell*, **7**, 503–512.
73. Rushton, E., Rohrbough, J., Deutsch, K. and Broadie, K. (2012) Structure-function analysis of endogenous lectin mind-the-gap in synaptogenesis. *Dev. Neurobiol.*, **72**, 1161–1179.
74. Rohrbough, J. and Broadie, K. (2002) Electrophysiological analysis of synaptic transmission in central neurons of *Drosophila* larvae. *J. Neurophysiol.*, **88**, 847–860.
75. Mathew, D., Ataman, B., Chen, J., Zhang, Y., Cumberledge, S. and Budnik, V. (2005) Wingless signaling at synapses is through cleavage and nuclear import of receptor DFrizzled2. *Science*, **310**, 1344–1347.